

Award Number:

W81XWH-12-1-0074

TITLE:

Dissecting and Targeting Latent Metastasis

PRINCIPAL INVESTIGATOR:

Joan Massagué, PhD

CONTRACTING ORGANIZATION:

**Sloan-Kettering Institute for Cancer Research
Memorial Sloan-Kettering Cancer Center**

New York, NY 10065

REPORT DATE:

September 2013

TYPE OF REPORT:

Annual

PREPARED FOR: U.S. Army Medical Research and Materiel Command
Fort Detrick, Maryland 21702-5012

DISTRIBUTION STATEMENT: (Check one)

Approved for public release; distribution unlimited

The views, opinions and/or findings contained in this report are those of the author(s) and should not be construed as an official Department of the Army position, policy or decision unless so designated by other documentation.

REPORT DOCUMENTATION PAGE

Form Approved
OMB No. 0704-0188

Public reporting burden for this collection of information is estimated to average 1 hour per response, including the time for reviewing instructions, searching existing data sources, gathering and maintaining the data needed, and completing and reviewing this collection of information. Send comments regarding this burden estimate or any other aspect of this collection of information, including suggestions for reducing this burden to Department of Defense, Washington Headquarters Services, Directorate for Information Operations and Reports (0704-0188), 1215 Jefferson Davis Highway, Suite 1204, Arlington, VA 22202-4302. Respondents should be aware that notwithstanding any other provision of law, no person shall be subject to any penalty for failing to comply with a collection of information if it does not display a currently valid OMB control number. **PLEASE DO NOT RETURN YOUR FORM TO THE ABOVE ADDRESS.**

1. REPORT DATE (DD-MM-YYYY) September 2013		2. REPORT TYPE Annual		3. DATES COVERED (From - To) 1September2012-31August2013	
4. TITLE AND SUBTITLE Dissecting and Targeting Latent Metastasis				5a. CONTRACT NUMBER	
				5b. GRANT NUMBER W81XWH-12-1-0074	
				5c. PROGRAM ELEMENT NUMBER	
6. AUTHOR(S) Joan Massague, PhD email:j-massague@ski.mskcc.org				5d. PROJECT NUMBER	
				5e. TASK NUMBER	
				5f. WORK UNIT NUMBER	
7. PERFORMING ORGANIZATION NAME(S) AND ADDRESS(ES) Sloan-Kettering Institute for Cancer Research New York, NY 10065				8. PERFORMING ORGANIZATION REPORT NUMBER	
9. SPONSORING / MONITORING AGENCY NAME(S) AND ADDRESS(ES) U.S. Army Medical Research And Material Command				10. SPONSOR/MONITOR'S ACRONYM(S)	
				11. SPONSOR/MONITOR'S REPORT NUMBER(S)	
12. DISTRIBUTION / AVAILABILITY STATEMENT Approved for public release; distribution unlimited					
13. SUPPLEMENTARY NOTES /					
14. ABSTRACT The overall goal of this project is to identify genes and pathways that support the viability of LMBC in host tissues. We have made progress under each of the three Tasks planned for year 01 in the original Statement of Work. Task 1 (to develop novel model systems of LMBC) has been fully accomplished in year 01, as planned. From triple-negative breast tumors and HER2-positive breast tumors we have derived cell lines that abundantly proliferate in vitro but have the capacity to enter a state of long-term latency after infiltrating target organs including lungs, the bone marrow, kidneys or the brain in mice. The resulting cell lines will be subjected to analysis during year 02 in order to decipher the genes and pathways that support LMBC cells in host tissues. Task 2 (to identify genes that support the viability of disseminated breast cancer cells), has been initiated in year 01 as planned. Progress includes the implementation of tagged ribosome affinity purification (TRAP) and, independently, the identification of genes that support the early survival of breast cancer cells that infiltrate the brain. Task 4 (to establish the functional relevance of LMBC genes and pathways) has also been initiated in year 01 as planned, with the identification of IGF1/CXCL12 signaling as an important mechanism for the initial survival of breast cancer cells that infiltrated the bone marrow. The studies and progress in the first year therefore represent highly promising progress towards the overall goal of delineating the biology of LMBC.					
15. SUBJECT TERMS Latent metastasis bone metastasis lung metastasis brain metastasis cancer cell survival vascular cooption in vivo imaging					
16. SECURITY CLASSIFICATION OF: U			17. LIMITATION OF ABSTRACT UU	18. NUMBER OF PAGES 77	19a. NAME OF RESPONSIBLE PERSON USAMRMC
a. REPORT U	b. ABSTRACT U	c. THIS PAGE U			19b. TELEPHONE NUMBER (include area code)

CONGRESSIONALLY DIRECTED MEDICAL RESEARCH PROGRAM**Award DOD W81XWH-12-1-0074****Principal Investigator: Joan Massagué, PhD****ANNUAL REPORT****TABLE OF CONTENTS**

	<u>Page</u>
Introduction.....	4
Body/Results.....	4
Key Research Accomplishments.....	9
Reportable Outcomes.....	9
Conclusion.....	10
References.....	11
Appendices.....	14
Supporting Data.....	15

INTRODUCTION

Metastasis is physically and psychologically devastating, frequently incurable, and the cause of 90% of deaths from breast cancer. Thousands of tumor cells may infiltrate the organs of a breast cancer patient before the primary tumor is diagnosed and removed. While the vast majority of these cells die, a residual population adopts a low-proliferation state that protects these cells from death. This population constitutes latent metastasis of breast cancer (LMBC), and it likely requires powerful mechanisms to survive long-term in the newly invaded microenvironments. This stress is compounded by the impact of therapy that the patient will receive after diagnosis. In spite of the obvious scientific interest of and medical importance of this problem, almost nothing is known about the cancer cell functions, host tissue signals, and physical niches that nurse the survival and fitness of cancer cells during LMBC. Progress has been hampered by a lack of model systems of latent metastasis in general and LMBC in particular. Developing and using experimental models of LMBC to elucidate these survival mechanisms will provide a basis for therapeutically targeting LMBC in order to prevent metastasis of breast cancer.

BODY / RESULTS

Progress under Task 1: To develop novel model systems of LMBC.

We sought to obtain disseminated tumor cells from human cancer cell lines representing cancers in which metastatic latency is clinically observed. Emphasis was placed on cell lines derived from HER2-positive breast cancer (HCC1954 cell line), triple-negative breast cancer (MDA231 and CN34 cell lines) and, for the purpose of comparative analysis of another type of cancer, lung adenocarcinoma (H2087 cell line). Tumor cells were labeled with GFP-luciferase to track them and with an antibiotic resistance gene (hygromycin/blastidicin) to isolate them from the mouse tissues. The labeled cells were injected into the left cardiac ventricle of athymic mice, which are deficient in T and B cells. Inoculation allowed the distribution of cancer cells throughout the body, as verified by imaging of the mice by bioluminescent imaging (BLI) 24 h after inoculation. Mice were monitored for two months. A few mice developed overt metastases during this period. These lesions were harvested and placed in culture for the isolation of aggressive metastatic cell line derivatives. Most mice however did not develop detectable metastasis over this two-month period, or developed a low level of BLI signals that remained stable and did not progress. We then harvested tissues of interest (brain, lung, liver, bone marrow, and kidney) to obtain tumor cells that were able to survive as micro-metastasis without forming overt metastasis. The isolated latent metastatic cells were expanded in culture, demonstrating that these cells have the capacity to actively proliferate under favorable conditions. We then re-injected the cells in mice to verify that these cells retain the capacity to engage in a low-cycling state after infiltrating target organs and to remain in this state for months except for the stochastic, low frequency generation of lethal macrometastatic lesion.

Progress Item 1.1. Using this approach, we have successfully isolated latent metastatic cells from breast and lung cancers (**Supporting Figure 1**). From the HER2-positive breast cancer cell line HCC1954 we isolated latency-competent derivatives that can populate the brain, bone marrow and lungs (HCC1954-LMBC1 cells). A more aggressive derivative (HCC1954-BrM) was also obtained. Latent bone metastasis derivatives were isolated from triple-negative breast cancer cell lines (MDA231-SCP6, and CN34-Bo-LMBC1), along with aggressive derivatives.

From the H2087 lung adenocarcinoma cell line we isolated latent lung and kidney metastatic cell derivatives (H2087-LMLC1), along with aggressively lung and bone metastatic derivatives.

It is interesting to note that although kidney metastasis is rare in lung cancer patients we did obtain latent kidney metastatic cells from the H2087, suggesting that latent metastatic cells can survive in sanctuary sites where they do not necessarily form overt metastases. These cells could eventually enter blood circulation and colonize target secondary sites. While isolating second-generation latent metastatic cells we detected occasional macro-metastases in the lungs, bones or brains of mice. These results indicate that the metastatic cell lines have the two key properties that we sought: (i) to be able to adopt a latent state after infiltrating target tissues, and (ii) to retain metastasis-initiating capabilities that can give rise to lethal lesions in vital organs. The above-described latent metastatic cell lines are being used to illuminate the molecular basis for the latent metastasis state.

Progress Item 1.2. In parallel with the isolation of these cell lines with latent metastatic capacity, we have developed sensitive qRT-PCR assays to detect low abundance disseminated cancer cells in mouse tissue (**Supporting Figure 2**). Using specific TaqMan probes for human $\beta 2$ -microglobulin (*B2M*) and *luciferase*, we can detect as few as 10 human cancer cells in mouse tissue. In mice with no BLI signal two months after injecting H2087-LMLC1, we were able to detect their existence by qRT-PCR. Additionally we optimized protocols to perform immunohistochemical analysis using GFP antibody on serially sectioned bone, brain, lung and kidneys in order to determine the number of disseminated cancer cells.

Progress under Task 2: Identify cell viability genes in disseminated breast cancer cells.

Metastasis is the main cause of death from cancer, but biologically metastasis is a rather inefficient process. Most cancer cells that leave a solid tumor perish, and much of this attrition happens as circulating cancer cells infiltrate distant organs [1]. Although mechanisms for early steps of tumor cell dispersion and for late stages of macrometastatic outgrowth are known [2,3], what factors determine the survival and adaptation of disseminated cancer cells in vital organs remain obscure. Identifying these factors is particularly critical in the case of brain metastasis. Brain relapse is the most devastating complication of cancer, with acute neurologic distress and high mortality as typical traits [4]. The incidence of brain metastasis is ten times higher than that of all primary brain tumors combined [5]. Breast cancer and lung cancer are the top sources of brain metastasis, together accounting for nearly two thirds of total cases. Melanoma, colorectal cancer, and renal cell carcinoma account for most of the rest [6]. However, it is in the brain that infiltrating cancer cells face a particularly high rate of attrition, as shown in experimental models [7]. Brain metastasis tends to be a late complication of cancer in the clinic [8,9] and is rare in mice with genetically engineered tumors that readily metastasize to other organs [10,11]. When brain metastasis eventually emerges though, the lesions are highly aggressive and resistant to therapy. This point is illustrated by the rising incidence of brain metastasis of HER2+ breast cancer, a disease in which antibodies targeting the HER2 oncoprotein are effective in controlling extracranial disease but not so against brain metastasis [12].

The severe attrition of metastatic cells in the brain and the late occurrence of brain metastasis in the clinic argue that circulating cancer cells face major hurdles in colonizing this organ. One

obstacle is the tight nature of the brain capillary walls, the blood-brain barrier (BBB). Cancer cells require specialized mechanisms to traverse the BBB, and molecular mediators of this process were recently identified [13,14]. However, most cancer cells that pass the BBB die [7,15] despite the presence of stromal and cell-autonomous activities that would favor tumor outgrowth [16-18]. Interestingly, cancer cells that succeed at infiltrating the brain present the striking feature of adhering to the surface of capillaries and growing as a furrow around the vessels, whereas those that fail to coopt the vasculature also fail to thrive [7,19,20]. What kills most cancer cells that pass through the BBB, and what enables the few survivors to coopt the vasculature are questions of biologic and clinical interest.

Progress Item 2.1. Seeking to define common mechanisms for metastatic colonization of the brain, we focused on a small set of genes whose expression is associated with brain metastatic phenotypes both in breast and in lung adenocarcinoma models [13,21]. One of these genes, *SERPINI1*, encoding the PA inhibitor neuroserpin, is normally expressed mainly in the brain. The plasminogen activators, tPA and uPA, convert plasminogen into plasmin, an endopeptidase that mediates fibrinolysis in blood clot resolution and is also involved in the stromal response to brain injury [22,23]. Reactive astrocytes are major sources of PAs in ischemia and neurodegenerative injury [24-26]. To avert the deleterious action of plasmin neurons express neuroserpin [27].

We found that neuroserpin and other closely related anti-PA serpins are selectively overexpressed in most experimental models and clinical samples of brain metastasis from lung and breast cancers (**refer to manuscript by Valiente et al in Appendix for supporting data**). We identified plasmin from the reactive brain stroma as a defense against metastatic invasion, and anti-PA serpins in cancer cells as a shield against this defense. Plasmin suppresses brain metastasis in two ways: by converting membrane-bound astrocytic FasL into a paracrine death signal for cancer cells, and by inactivating the axon pathfinding molecule L1CAM that metastatic cells express for spreading along brain capillaries and for metastatic outgrowth. Brain metastatic cells from lung cancer and breast cancer express high levels of anti-PA serpins, including neuroserpin and serpin B2, to prevent plasmin generation and its deleterious consequences. By protecting cancer cells from death signals and fostering vascular cooption, anti-PA serpins provide a unifying mechanism for the initiation of brain metastasis in lung and breast cancers.

The molecular mechanisms that we have defined protect metastatic cells from selective pressures that are particularly acute in the brain. However, a high mortality of infiltrating cancer cells is characteristic of metastasis in general [3,28], and vascular cooption occurs in metastasis to other organs and by other types of cancer [29-31]. Vascular cooption also provides cancer cells with an escape from therapy-induced hypoxia [31]. The anti-PA serpins that are up-regulated in our brain metastatic models are also expressed, albeit at lower levels, in counterparts metastatic to other organs. Moreover, L1CAM expression in primary tumors is associated with poor prognosis in various types of cancer, as are PA, plasmin, and FasL. The reactive brain stroma, with its high capacity to generate PA-plasmin and FasL, may be more challenging to infiltrating cancer cells than is the stroma in other organs and, as a result, it may select for accentuated versions of otherwise general metastatic traits. Although anti-PA serpins, plasmin, FasL and L1CAM had not been previously connected to metastatic cell survival and vascular cooption, their repeated

clinical association with poor prognosis and the mechanistic links established in the present work may reflect a wider role in cancer than we have demonstrated here.

Progress Item 2.2. A key question in understanding the origin of metastasis is how cancer cells in a primary tumor acquire the ability to colonize a particular distant organ. Cancer-associated fibroblasts (CAFs) in triple-negative (TN) breast tumors skew heterogeneous cancer cell populations towards a predominance of clones that thrive on the CAF-derived factors CXCL12 and IGF1. Limiting concentrations of these factors select for cancer cells with high Src activity, a known clinical predictor of bone relapse and an enhancer of PI3K-Akt pathway activation by CXCL12 and IGF1. Carcinoma clones selected in this manner are primed for metastasis in the CXCL12-rich microenvironment of the bone marrow. The evidence suggests that stromal signals resembling those of a distant organ select for cancer cells that are primed for metastasis in that organ, thus illuminating the evolution of metastatic traits in a primary tumor and its distant metastases.

In the context of these studies we implemented translating ribosome affinity purification (TRAP) to assess whether mesenchymal stem cell (MSC) supplementation would recapitulate the key features of human CAF⁺ breast tumors (**Supporting Figure 3**). To transcriptionally profile cancer cells in MSC-supplemented experimental tumors in situ we engineered metastatic breast cancer cells with a ribosomal protein L10a fused to enhanced green fluorescent protein (EGFP-L10a). The expressed EGFP-L10a is incorporated into the cancer cell ribosomes, allowing the specific retrieval of cancer cell transcripts from tumor lysates by polysome immunoprecipitation with anti-EGFP antibody. This technique of TRAP [32] enables RNA-seq analysis of the cancer cell transcriptome from freshly excised tumors without intervening cell isolation steps that could confound the results.

MDA231 cells expressing EGFP-L10a were implanted alone as a control, or MDA231 admixed with MSCs at a 1:1 ratio into the mammary fat pads of mice. RNA-seq analysis of the TRAP samples showed that tumor supplementation with MSCs caused a transcriptomic shift in the cancer cells that resembled the shift associated with CAF⁺ status in clinical tumor samples. Consistently, MSC-supplemented tumors showed a 3- to 10-fold increase in the proportion of cells staining positive for the CAF marker alpha-SMA, and a higher level of CXCL12 and IGF1 immunostaining. The TRAP RNA-seq data revealed no ribosome-associated CXCL12 or IGF1 transcripts in cancer cells.

The gene expression profile of cancer cells from MSC-supplemented tumors resembled the profile of MDA231 cells treated with limiting CXCL12 and IGF1 concentrations. This similarity was further validated by Ingenuity pathway analysis of the differentially expressed genes. Upstream regulator analysis revealed CXCL12- and IGF1-induced signaling and their downstream PI3K-Akt signaling in the cancer cells. These genes are enriched in biological processes associated with metastasis and bone biology. Thus, the model tumors co-transplanted with MSCs gained a bioactive CXCL12/IGF1 microenvironment and response features that are characteristic of CAF⁺ TN tumors.

Progress under Task 4: Establish the functional relevance of LMBC genes and pathways.

Progress Item 4.1. We initiated our work under this task by functionally validating in mouse models of breast cancer the relevance of the CXCL12/IGF1-dependent PI3K-AKT signaling pathway in the seeding of bone marrow metastasis (**Supporting Figure 4**). Cancer cells were purified from MDA231 mammary tumors, expanded in culture for several passages, and characterized. Cancer cells recovered from MSC-supplemented tumors showed a high level of pY416-Src compared to populations derived from control tumors. Treatment of the mice with inhibitors of the CXCL12 receptor CXCR4 (AMD3100) [33] and of the IGF1 receptor IGF1R (BMS754807) during tumor growth prevented the accumulation of pY416-Src-high cells, without significantly affecting overall tumor growth. Importantly, cancer cell populations derived from the MSC-supplemented tumors were significantly more metastatic to bone, without a gain in lung colonizing ability.

Cancer cell populations derived from mice treated with IGF1R and CXCR4 inhibitors were poorly metastatic to bone. To confirm the specificity of these effects, we knocked down CXCR4 and IGF1R simultaneously in MDA231 cells. Knockdown of the two receptors did not affect the level of pY416-Src in MDA231 cells but it prevented MSCs from selecting for carcinoma clones with high pY416-Src content. Furthermore, primary CAFs isolated from a human breast tumor secreted CXCL12 and IGF1 (12.6 ± 0.2 ng/ml and 0.44 ± 0.02 ng/ml, respectively after 96 h in culture) and selected for a pY416-Src enriched cancer cell population when admixed with MDA231 cells forming mammary tumors in mice. The evidence therefore supports a model in which CAFs in mammary tumors cause an accumulation of stromal CXCL12 and IGF1, and these factors act directly on cancer cells to drive the selection of Src-hyperactive clones that are automatically primed for adaptation to the bone metastatic microenvironment.

KEY RESEARCH ACCOMPLISHMENTS

- Isolation of latent metastatic cells from breast and lung cancers.
- Development of sensitive qPCR assays and IHC protocols to detect low abundance disseminated cancer cells in the mouse tissue.
- Identification of plasmin from the reactive brain stroma as a defense against metastatic breast cancer invasion, and anti-PA serpins in cancer cells as a shield against this defense.
- Identification of FasL as a key astrocyte-derived signal that kills infiltrating breast cancer cells in the brain.
- Identification of the axon pathfinding molecule L1CAM in breast cancer cells as a mediator of spreading along brain capillaries and for vascular cooption by latent cancer cells and the initiation of metastatic colonization.
- Implementation of translating ribosome affinity purification (TRAP) for transcriptional analysis of selected cancer cell populations in highly heterogeneous tumor microenvironments.
- Functional validation of CXCL12/IGF1-dependent PI3K-AKT signaling in the initial survival of metastatic breast cancer cells that infiltrate the bone marrow.

REPORTABLE OUTCOMES

Manuscript:

Valiente, M., Obenauf, A.C., Jin, X., Chen, Q., Zhang, X.H.F., Lee, D.J., Chaft, J.E., Kris, M.G., Huse, J.T., Brogi, E. and Massagué, J. Serpins promote cancer cell survival and vascular cooption in brain metastasis. *Submitted for publication*

Presentations:

SEBBM Conference–Plenary Lecture–Congress IUBMB-FEBS, Seville	9/4/2012
Starr Cancer Consortium Retreat-Cold Spring Harbor, New York	9/25/2012
Ted Couch Lecture - Moffitt Cancer Center, Florida	9/28/2012
Harvard Med. School & Mass. General Hospital	10/4/2012
NCRI Conference, Plenary Lecture - Liverpool, UK	11/3/2012
Uppsala University, Plenary Lecture - Sweden	11/5/2012
UT Southwestern, University Lecture Series	1/18/2013
AACR Special Conference Session Chairperson & Speaker “Tumor Invasion & Metastasis Meeting”, San Diego	1/25/2013
Fox Chase Cancer Center, Distinguished Lecture Series, Phil. PA	2/18/2013
HHMI Annual Science Meeting, Maryland	3/5/2013
NIH WALS Lecture - Bethesda, MA NIH WALS	4/5/2013
2013 AACR Annual Meeting–Co-Chairperson “Genetic Determinants of Brain Metastasis” Washington, DC	4/17/2013
Roswell Park Cancer Institute, Buffalo, NY	5/23/2013
EuroCancer – Keynote Lecture- Paris	7/30/2013

Cell lines: HCC1954-LMBC1, HCC1954-BrM, H2087-LMLC1

CONCLUSION

The overall goals of this project are to biologically dissect, molecularly deconstruct, and conceptually understand LMBC, in order to target its viability for the prevention of metastasis. Our progress towards this goal is right on schedule. We have accomplished the tasks that were scheduled for the period of this Progress Report without encountering major unforeseen difficulties. The first specific task of this project to develop transplantable LMBC model systems has been successfully accomplished, thus enabling the rest of the project to proceed. Using innovative technologies, we have isolated LMBC cells and are now proceeding with molecular and functional analysis to identify the basis for the latent metastasis capacity of these cells. By pioneering the molecular and functional dissection of LMBC we will identify its vulnerabilities and enable the design of new treatments to prevent metastasis. Through innovation and new progress we hope to demonstrate that LMBC is a tractable problem and encourage other investigators to join in this effort.

REFERENCES

1. Chambers, A.F., Groom, A.C., and MacDonald, I.C., 2002. Dissemination and growth of cancer cells in metastatic sites. *Nature Reviews: Cancer* 2: 563-72.
2. Vanharanta, S. and Massague, J., 2013. Origins of metastatic traits. *Cancer Cell* 24: 410-21.
3. Valastyan, S. and Weinberg, R.A., 2011. Tumor metastasis: molecular insights and evolving paradigms. *Cell* 147: 275-92.
4. Gavrilovic, I.T. and Posner, J.B., 2005. Brain metastases: epidemiology and pathophysiology. *Journal of Neuro-Oncology* 75: 5-14.
5. Maher, E.A., Mietz, J., Arteaga, C.L., DePinho, R.A., and Mohla, S., 2009. Brain metastasis: opportunities in basic and translational research. *Cancer Research* 69: 6015-20.
6. Barnholtz-Sloan, J.S., Sloan, A.E., Davis, F.G., Vigneau, F.D., Lai, P., and Sawaya, R.E., 2004. Incidence proportions of brain metastases in patients diagnosed (1973 to 2001) in the Metropolitan Detroit Cancer Surveillance System. *Journal of Clinical Oncology* 22: 2865-72.
7. Kienast, Y., von Baumgarten, L., Fuhrmann, M., Klinkert, W.E., Goldbrunner, R., Herms, J., and Winkler, F., 2010. Real-time imaging reveals the single steps of brain metastasis formation. *Nature Medicine* 16: 116-22.
8. Feld, R., Rubinstein, L.V., and Weisenberger, T.H., 1984. Sites of recurrence in resected stage I non-small-cell lung cancer: a guide for future studies. *Journal of Clinical Oncology* 2: 1352-8.
9. Karrison, T.G., Ferguson, D.J., and Meier, P., 1999. Dormancy of mammary carcinoma after mastectomy. *Journal of the National Cancer Institute* 91: 80-5.
10. Winslow, M.M., Dayton, T.L., Verhaak, R.G., Kim-Kiselak, C., Snyder, E.L., Feldser, D.M., Hubbard, D.D., DuPage, M.J., Whittaker, C.A., Hoersch, S., Yoon, S., Crowley, D., Bronson, R.T., Chiang, D.Y., Meyerson, M., and Jacks, T., 2011. Suppression of lung adenocarcinoma progression by Nkx2-1. *Nature* 473: 101-4.
11. Francia, G., Cruz-Munoz, W., Man, S., Xu, P., and Kerbel, R.S., 2011. Mouse models of advanced spontaneous metastasis for experimental therapeutics. *Nature Reviews: Cancer* 11: 135-41.
12. Lin, N.U. and Winer, E.P., 2007. Brain metastases: the HER2 paradigm. *Clinical Cancer Research* 13: 1648-55.
13. Bos, P.D., Zhang, X.H., Nadal, C., Shu, W., Gomis, R.R., Nguyen, D.X., Minn, A.J., van de Vijver, M.J., Gerald, W.L., Foekens, J.A., and Massagué, J., 2009. Genes that mediate breast cancer metastasis to the brain. *Nature* 459: 1005-9.
14. Li, B., Wang, C., Zhang, Y., Zhao, X.Y., Huang, B., Wu, P.F., Li, Q., Li, H., Liu, Y.S., Cao, L.Y., Dai, W.M., Fang, W.G., Shang, D.S., Cao, L., Zhao, W.D., and Chen, Y.H., 2013. Elevated PLGF contributes to small-cell lung cancer brain metastasis. *Oncogene* 32: 2952-2962.
15. Heyn, C., Ronald, J.A., Ramadan, S.S., Snir, J.A., Barry, A.M., MacKenzie, L.T., Mikulis, D.J., Palmieri, D., Bronder, J.L., Steeg, P.S., Yoneda, T., MacDonald, I.C., Chambers, A.F., Rutt, B.K., and Foster, P.J., 2006. In vivo MRI of cancer cell fate at the single-cell level in a mouse model of breast cancer metastasis to the brain. *Magnetic Resonance in Medicine* 56: 1001-10.

16. Kim, S.J., Kim, J.S., Park, E.S., Lee, J.S., Lin, Q., Langley, R.R., Maya, M., He, J., Kim, S.W., Weihua, Z., Balasubramanian, K., Fan, D., Mills, G.B., Hung, M.C., and Fidler, I.J., 2011. Astrocytes upregulate survival genes in tumor cells and induce protection from chemotherapy. *Neoplasia* 13: 286-98.
17. Nguyen, D.X., Bos, P.D., and Massagué, J., 2009. Metastasis: from dissemination to organ-specific colonization. *Nature Reviews: Cancer* 9: 274-84.
18. Seike, T., Fujita, K., Yamakawa, Y., Kido, M.A., Takiguchi, S., Teramoto, N., Iguchi, H., and Noda, M., 2011. Interaction between lung cancer cells and astrocytes via specific inflammatory cytokines in the microenvironment of brain metastasis. *Clinical & Experimental Metastasis* 28: 13-25.
19. Loriger, M. and Felding-Habermann, B., 2010. Capturing changes in the brain microenvironment during initial steps of breast cancer brain metastasis. *American Journal of Pathology* 176: 2958-71.
20. Carbonell, W.S., Anson, O., Sibson, N., and Muschel, R., 2009. The vascular basement membrane as "soil" in brain metastasis. *PloS one* 4: e5857.
21. Nguyen, D.X., Chiang, A.C., Zhang, X.H., Kim, J.Y., Kris, M.G., Ladanyi, M., Gerald, W.L., and Massagué, J., 2009. WNT/TCF signaling through LEF1 and HOXB9 mediates lung adenocarcinoma metastasis. *Cell* 138: 51-62.
22. Benarroch, E.E., 2007. Tissue plasminogen activator: beyond thrombolysis. *Neurology* 69: 799-802.
23. Sofroniew, M.V. and Vinters, H.V., 2010. Astrocytes: biology and pathology. *Acta Neuropathologica. Supplement* 119: 7-35.
24. Adhami, F., Yu, D., Yin, W., Schloemer, A., Burns, K.A., Liao, G., Degen, J.L., Chen, J., and Kuan, C.Y., 2008. Deleterious effects of plasminogen activators in neonatal cerebral hypoxia-ischemia. *American Journal of Pathology* 172: 1704-16.
25. Teesalu, T., Hinkkanen, A.E., and Vaheri, A., 2001. Coordinated induction of extracellular proteolysis systems during experimental autoimmune encephalomyelitis in mice. *American Journal of Pathology* 159: 2227-37.
26. Ganesh, B.S. and Chintala, S.K., 2011. Inhibition of reactive gliosis attenuates excitotoxicity-mediated death of retinal ganglion cells. *PloS one* 6: e18305.
27. Yepes, M., Sandkvist, M., Wong, M.K., Coleman, T.A., Smith, E., Cohan, S.L., and Lawrence, D.A., 2000. Neuroserpin reduces cerebral infarct volume and protects neurons from ischemia-induced apoptosis. *Blood* 96: 569-76.
28. Gupta, G.P. and Massagué, J., 2006. Cancer metastasis: building a framework. *Cell* 127: 679-95.
29. Blouw, B., Song, H., Tihan, T., Bosze, J., Ferrara, N., Gerber, H.P., Johnson, R.S., and Bergers, G., 2003. The hypoxic response of tumors is dependent on their microenvironment. *Cancer Cell* 4: 133-46.
30. Leenders, W.P., Kusters, B., and de Waal, R.M., 2002. Vessel co-option: how tumors obtain blood supply in the absence of sprouting angiogenesis. *Endothelium* 9: 83-7.
31. Leenders, W.P., Kusters, B., Verrijp, K., Maass, C., Wesseling, P., Heerschap, A., Ruiter, D., Ryan, A., and de Waal, R., 2004. Antiangiogenic therapy of cerebral melanoma metastases results in sustained tumor progression via vessel co-option. *Clinical Cancer Research* 10: 6222-30.
32. Heiman, M., Schaefer, A., Gong, S., Peterson, J.D., Day, M., Ramsey, K.E., Suarez-Farinas, M., Schwarz, C., Stephan, D.A., Surmeier, D.J., Greengard, P., and Heintz, N.,

2008. A translational profiling approach for the molecular characterization of CNS cell types. *Cell* 135: 738-48.
33. Hatse, S., Princen, K., Bridger, G., De Clercq, E., and Schols, D., 2002. Chemokine receptor inhibition by AMD3100 is strictly confined to CXCR4. *FEBS Lett* 527: 255-62.

APPENDIX

Manuscript: Valiente, M., Obenauf, A.C., Jin, X., Chen, Q., Zhang, X.H.F., Lee, D.J., Chaff, J.E., Kris, M.G., Huse, J.T., Brogi, E. and Massagué, J. Serpins promote cancer cell survival and vascular cooption in brain metastasis. *Submitted for publication*

Serpins Shield Brain Metastatic Cells from Death Signals and Vascular Detachment

Manuel Valiente¹, Anna C. Obenauf¹, Xin Jin¹, Qing Chen¹, Xiang H.-F. Zhang^{1,8}, Derek
J. Lee¹, Jamie E. Chaff², Mark G. Kris², Jason T. Huse^{3,4}, Edi Brogi⁵ and Joan
Massagué^{1,4,6,7}

¹ Cancer Biology and Genetics Program

² Department of Medicine

³ Human Oncology and Pathogenesis Program

⁴ Brain Tumor Center

⁵ Department of Pathology

⁶ Metastasis Research Center

Memorial Sloan-Kettering Cancer Center, New York, NY 10065, USA

⁷ Howard Hughes Medical Institute, Chevy Chase, MD 21205, USA

⁸ Present address: Lester and Sue Smith Breast Center, Baylor College of Medicine,
One Baylor Plaza, Houston, TX 77030, USA

Correspondence:

Joan Massagué, PhD
Box 116, Memorial Sloan-Kettering Cancer Center
1275 York Avenue, New York, NY 10065 USA
Phone: 646-888-2044 Email: j-massague@ski.mskcc.org

ABSTRACT

Brain metastasis is an ominous complication of cancer, yet most cancer cells that infiltrate the brain die of unknown causes. Here we identify plasmin from the reactive brain stroma as a defense against metastatic invasion, and plasminogen activator (PA) inhibitory serpins in cancer cells as a shield against this defense. Plasmin suppresses brain metastasis in two ways: by converting membrane-bound astrocyte FasL into a paracrine death signal for cancer cells, and by inactivating the axon pathfinding molecule L1CAM that metastatic cells express for binding to brain capillaries and for metastatic outgrowth. Brain metastatic cells from lung cancer and breast cancer express high levels of anti-PA serpins, including neuroserpin and serpin B2, to prevent plasmin generation and its deleterious consequences. By protecting cancer cells from death signals and fostering vascular cooption, anti-PA serpins provide a unifying mechanism for the initiation of brain metastasis in lung and breast cancers.

INTRODUCTION

Metastasis is the main cause of death from cancer, but biologically metastasis is a rather inefficient process. Most cancer cells that leave a solid tumor perish, and much of this attrition happens as circulating cancer cells infiltrate distant organs (Chambers et al., 2002; Fidler, 2003; Nguyen et al., 2009a; Schreiber et al., 2011; Valastyan and Weinberg, 2011). Even cell lines that were experimentally enriched for metastasis-initiating activity suffer severe attrition in the organs they invade. The scarcity of survival signals in the host parenchyma, lack of a supportive stroma for cancer stem cells, and an overexposure to innate immunity are postulated causes of elimination of disseminated cancer cells. Although recent work revealed mechanisms for early steps of tumor cell dispersion and for late stages of macrometastatic outgrowth (Valastyan and Weinberg, 2011; Vanharanta and Massagué, 2013), what factors determine the survival and adaptation of disseminated cancer cells in vital organs remain unknown.

Identifying these factors is particularly critical in the case of brain metastasis. Brain relapse is the most devastating complication of cancer, with acute neurologic distress and high mortality as typical traits (Gavrilovic and Posner, 2005; Lutterbach et al., 2002). The incidence of brain metastasis is ten times higher than that of all primary brain tumors combined, and is on the rise (Maher et al., 2009). Lung cancer and breast cancer are the top sources of brain metastasis, together accounting for nearly two thirds of cases. Melanoma, colorectal cancer, and renal cell carcinoma account for most of the rest (Barnholtz-Sloan et al., 2004; Schouten et al., 2002). However, it is in the brain that infiltrating cancer cells face a particularly high rate of attrition, as shown in experimental models (Heyn et al., 2006; Kienast et al., 2010; Perera et al., 2012; Steeg et al., 2011). In line with this phenomenon, brain metastasis tends to be a late complication of cancer in the clinic (Feld et al., 1984; Karrison et al., 1999; Schmidt-Kittler et al., 2003) and is rare in mice with genetically engineered tumors that readily metastasize to other organs (Francia et al., 2011; Meuwissen et al., 2003; Moody et al., 2002; Regales et al., 2009; Siegel et al., 2003; Winslow et al., 2011). When brain metastasis eventually emerges, the lesions are highly aggressive and resistant to therapy. This point is dramatically illustrated by the current rise in the incidence of brain metastasis of HER2+ breast cancer, a disease in which antibodies targeting the HER2 oncoprotein are effective in

controlling extracranial disease but not so against brain metastasis (Leyland-Jones, 2009; Lin and Winer, 2007; Palmieri et al., 2007; Sledge, 2011; Stemmler et al., 2006).

The severe attrition of metastatic cells in the brain and the late occurrence of brain metastasis in the clinic argue that circulating cancer cells face major hurdles in colonizing this organ. One obstacle is the tight nature of the brain capillary walls, the blood-brain barrier (BBB). Cancer cells require specialized mechanisms to traverse the BBB, and molecular mediators of this process were recently identified (Bos et al., 2009; Li et al., 2013). However, most cancer cells that pass the BBB die (Heyn et al., 2006; Kienast et al., 2010; Perera et al., 2012; Steeg et al., 2011) despite the presence of stromal signals and cell-autonomous activities that would favor cell proliferation (Kim et al., 2011; Nguyen et al., 2009a; Qian et al., 2011; Seike et al., 2011). Interestingly, cancer cells that succeed at infiltrating the brain present the striking feature of adhering to the surface of brain capillaries and growing as a furrow around the vessels. Cancer cells that fail to coopt the vasculature in this manner also fail to thrive (Kienast et al., 2010). What kills a majority of cancer cells that pass through the BBB, and what enables the few cells that survive to coopt the vasculature are questions of biologic and clinical interest.

Seeking to define common mechanisms for metastatic colonization of the brain, we focused on a small set of genes whose expression is associated with brain metastatic phenotypes both in lung and in breast adenocarcinoma models. We were intrigued that one of these genes, *SERPINI1*, encoding the PA inhibitor neuroserpin, is normally expressed mainly in the brain. The plasminogen activators, tPA and uPA, convert plasminogen into plasmin, an endopeptidase that mediates fibrinolysis in blood clot resolution and is also involved in the stromal response to brain injury (Benarroch, 2007; Sofroniew and Vinters, 2010). Reactive astrocytes are major sources of PAs in ischemia and neurodegenerative injury (Adhami et al., 2008; Ganesh and Chintala, 2011; Teesalu et al., 2001). To avert the deleterious action of plasmin neurons express neuroserpin (Yepes et al., 2000). We found that neuroserpin and other closely related anti-PA serpins are selectively overexpressed in most experimental models and clinical samples of brain metastasis from lung and breast cancers. By secreting PA inhibitory serpins brain metastatic cells thwart the lethal action of plasmin from the reactive stroma. We further show that suppression of Fas-mediated cancer cell killing and promotion of

L1CAM-mediated vascular cooption lie downstream of anti-PA serpin action as critical requirements for the initiation of metastasis in the brain.

RESULTS

Association of PA-inhibitory serpins with the brain metastatic phenotype

In order to identify shared mediators of brain metastasis we analyzed transcriptomic signatures of brain metastatic subpopulations (BrM) that were isolated from lymph node-derived human lung adenocarcinoma cell lines H2030 and PC9 (Nguyen et al., 2009b) and from pleural effusion-derived breast cancer cell lines MDA-MB-231 (MDA231 for short) and CN34 (Bos et al., 2009) (Figure 1A). Seven genes were upregulated in brain metastatic cells compared to the source parental lines in at least three of the four models (Figure S1A). Among these genes, *LEF1* was previously defined as a mediator of WNT signaling in brain metastasis by lung adenocarcinoma cells (Nguyen et al., 2009b). *SERPINI1* (see below), but none of the other genes, was associated with brain relapse in human primary tumors. *SERPINI1*, encoding neuroserpin (NS), was also intriguing because its expression is normally restricted to neurons, where it protects from PA-related cytotoxicity (Fabbro and Seeds, 2009; Yepes et al., 2000).

The serpin family in human comprises 36 members that collectively target 18 proteases (Irving et al., 2000). Four of these serpins –neuroserpin and serpins B2, E1, and E2– selectively inhibit PA (Law et al., 2006). Gene expression analysis using qRT-PCR showed that three of the anti-PA serpins were upregulated >3-fold at the mRNA level in brain metastatic cells (Figure 1A). Only one other serpin, *SERPIND1*, was also upregulated (Figure 1A). Serpin D1 inhibits thrombin, which cooperates with plasminogen in cerebral injury (Fujimoto et al., 2008). Bone metastatic derivatives (MDA231-BoM) (Kang et al., 2003) and lung metastatic derivatives (MDA231-LM2) (Minn et al., 2005) were available for comparisons with MDA231-BrM2, and showed little (BoM) or no upregulation (LM2) of the serpins (Figure 1B).

To investigate immune competent models, and a different subtype of breast cancer, we established the cell line ErbB2-P from a mouse mammary tumor driven by a mutant *ErbB2* transgene (Muller et al., 1988) and then isolated a brain metastatic derivative (ErbB2-BrM2) by in vivo selection of ErbB2-P in congenic mice. ErbB2-BrM2 cells showed a strong upregulation of serpins B2 and D1 compared to the parental line (Figure 1A). We also screened four cell lines derived from lymph node metastases of genetically engineered *Kras*^{G12D};*p53*^{-/-} mouse lung adenocarcinomas (Winslow et al.,

2011). All four lines were highly metastatic to visceral organs but ranged widely in brain metastatic activity (Figures 1C, S1B); brain metastasis was associated with high expression of serpins I1, B2, E2 and/or D1 (Figure 1C,D).

The upregulation of neuroserpin and serpin B2 in brain metastatic cells was confirmed at the protein level (Figure S1C,D). Moreover, conditioned media from brain metastatic cell lines inhibited the conversion of plasminogen into plasmin, as determined using a chromogenic plasmin activity assay (Bai et al., 2011) (Figures 1E,F and S1E). The only exception was PC9-BrM3, a cell line that is less aggressive in brain metastasis compared to H2030-BrM3 (Nguyen et al., 2009b) and lacks upregulated anti-PA serpins (Figure 1A, S1C,D).

Neuroserpin and serpin B2 in human brain metastasis tissues

Focusing on the two most frequently upregulated anti-PA serpins in these models, neuroserpin and serpin B2, we queried gene-expression data from 106 primary lung adenocarcinomas with relapse annotation (Nguyen et al., 2009b). The expression level of *SERPINI1* and *SERPINB2* in the tumors was associated with brain relapse, both as individual genes (data not shown) and combined ($p = 0.018$, hazard ratio = 2.33 +/- 0.3; Figure 1G). Expression of the two genes was not significantly associated with metastasis to bone or lungs ($p = 0.89$, hazard ratio = 0.91 +/- 0.33; $p = 0.36$, hazard ratio = 0.76 +/- 0.27; Figure S1F,G). *SERPINI1* and *SERPINB2* expression in primary breast tumors was not a predictor of brain metastasis ($p = 0.21$, hazard ratio = 0.96 +/- 0.16; Figure S1H), though in most of these cases brain relapse was a late event.

We performed immunohistochemical analysis of neuroserpin and serpin B2 in human brain metastasis tissue, using as a reference brain lesions formed by serpin-expressing human cancer cells in mice (Figure S1I). Among 33 brain metastases of non-small cell lung carcinomas, 45% scored positive for neuroserpin and 94% for serpin B2. Among 123 from breast cancer of various subtypes, 77% scored positive for neuroserpin and 34% for serpin B2 (Figures 1H,I and S1I,J). The immunoreactivity was diffusely distributed in the cytoplasm of carcinoma cells and only minimally in the scant extracellular stroma. Positivity for neuroserpin and serpin B2 in the peritumoral inflammatory infiltrate was limited.

Plasmin is lethal to cancer cells that invade the brain parenchyma

The MDA231-BrM2 or H2030-BrM3 models are metastatic to the brain both from orthotopic tumors and from the arterial circulation (Bos et al., 2009; Nguyen et al., 2009b). We inoculated these cells into the arterial circulation of immunodeficient mice via the left cardiac ventricle and fixed the tissue to count cancer cells lodged in the brain capillary network at different time points (Figures 2A-C, S2A). One day after inoculation, we observed isolated cancer cells trapped within brain capillaries (Figure 2B, and H2030-BrM3 data not shown). Cells passing through the BBB were observed between days 2 and 7 after inoculation (Figures 2B, S2B). All cells remaining within capillaries on day 7 stained positive for the apoptosis marker, cleaved caspase-3 (Figure S2C,D) and disappeared thereafter. In parental MDA231 the number of extravasated cells dropped sharply after day 5 and rarely recovered (Figure S2B). In line with previous reports (Carbonell et al., 2009; Chambers, 2000; Kienast et al., 2010; Loriger and Felding-Habermann, 2010), >90% of cancer cells entering the brain disappeared within days. In MDA231-BrM2 the number of extravasated cells increased until day 7, dropped sharply by day 10, but recovered by day 16. The survivors were bound to and stretched over the abluminal surface of brain capillaries (Figure 2A,B). Outgrowth mainly occurred on the coopted vessels (Figure 2C, summarized in Figure 2D)

In the brain, metastatic cells were in close proximity to astrocytes (Figures 2E, S2E,F), microglia and neurons (Figure S2G-J). Reactive astrocytes, identified by GFAP overexpression and a stellate morphology, were associated with cancer cells right after extravasation (day 3) and thereafter (Figures 2E, S2E,F). As reactive astrocytes are a major source of PA in brain injury (Adhami et al., 2008; Fabbro and Seeds, 2009; Ganesh and Chintala, 2011), we asked whether these cells were a source of PA in brain metastasis. Mouse brain sections harboring metastatic cells showed tPA and uPA immunoreactivity associated with astrocytes (Figures 2F,G). Mouse astrocytes in culture were superior to microglia at converting plasminogen into plasmin (Figure S2K). Neurons are known to produce plasminogen for neurite and synapse formation (Gutierrez-Fernandez et al., 2009; Hoover-Plow et al., 2001). We confirmed an association of plasminogen immunoreactivity with NeuN+ neurons surrounding metastatic cells in mouse brain (Figure 2H). Thus, the brain metastasis microenvironment contains the necessary components for plasmin production.

To determine whether plasmin in the brain parenchyma is harmful to metastatic cells we used mouse brain slices in culture (Figure 2I). When placed on top of brain slices

H2030-BrM3 cells migrated into the tissue, targeted blood capillaries, and spread on the surface of the vessels (Figure 2J). H2030-BrM3 cells survived and proliferated under these conditions (Figure 2K,L), whereas parental H2030 did not proliferate (Figure 2K,L) and underwent apoptosis (Figure 2M,N). Similar results were obtained with MDA231 cells (Figure S2M). In co-cultures of cancer cells with astrocytes and microglia, plasminogen addition triggered apoptosis in parental H2030 but not in H2030-BrM3 (Figure S2L). The brain tissue slices contained endogenous plasmin activity, and addition of the plasmin inhibitor α 2-antiplasmin (Bajou et al., 2008) inhibited this activity (Figure S2N,O). Addition of α 2-antiplasmin increased the survival of parental H2030 cells in brain slices (Figure 2K-N). Of note, addition of plasmin to cancer cell monolayer cultures did not trigger apoptosis (Figure S2P). These results suggested that plasmin, acting through unknown substrates in the brain microenvironment, kills infiltrating cancer cells, whereas highly metastatic cells are shielded from this threat (Figure 2O).

Neuroserpin protects metastatic cells from plasmin-mediated attrition

To investigate the role of neuroserpin in brain metastasis we first used the H2030-BrM3 model, in which only this serpin is upregulated (refer to Figure 1A). Brain lesions formed by H2030-BrM3 cells in mice showed strong neuroserpin immunoreactivity (Figure S3A). Two shRNAs that decreased neuroserpin expression and secretion by >85% (Figure S3B,C) did not affect the growth of H2030-BrM3 cells in culture (Figure S3D) but inhibited the metastatic activity of these cells, as shown by bioluminescence imaging (BLI) of marker luciferase in-vivo (Figure 3A-D), BLI ex-vivo (Figures 3B), and marker green fluorescent protein (GFP) expression in brain sections (Figure 3E). Neuroserpin depletion in H2030-BrM3 caused a significant drop in the number and size of brain lesions (Figures 3F, S3E), with a >90% overall reduction in brain tumor burden (Figure 3G). The few macroscopic lesions that developed were rich in neuroserpin (Figure S3F), indicating that these lesions grew from cells that escaped the knockdown.

Neuroserpin knockdown did not inhibit the extravasation of H2030-BrM3 cells into the brain parenchyma (Figure S3G). It also did not affect the ability of these cells to cross an endothelial/astrocyte BBB-like barrier in vitro, whereas the knockdown of *ST6Gal/NaC5*, a mediator of BBB extravasation (Bos et al., 2009), did (Figure S3H,I). In brain slice assays, neuroserpin knockdown in H2030-BrM3 cells decreased the number of infiltrated cells (Figure 3H,I) and increased apoptosis (Figure 3H,J), whereas overexpression of

neuroserpin in parental H2030 and MDA231 cells had the opposite effects (Figure 3K,L). In sum, neuroserpin expression in cancer cells supported their survival and outgrowth in the brain parenchyma.

Brain metastasis mediated by the PA inhibitory function of neuroserpin

To determine whether neuroserpin can increase the brain metastatic activity of lung cancer cells in vivo we used the PC9-BrM3 model. PC9-BrM3 cells can infiltrate the brain but are less aggressive than H2030-BrM3 (Nguyen et al., 2009b) and do not show upregulation of anti-PA serpins (refer to Figure 1A, S1C,D). PC9-BrM3 cells were stably transduced with vectors encoding the wild type neuroserpin or a mutant (neuroserpin Δ loop) that is devoid of PA inhibitory function (Takehara et al., 2009) (Figure S3J-L). The wild type neuroserpin significantly increased the brain metastatic activity of PC9-BrM3 cells whereas the mutant neuroserpin did not (Figure 3M,N) without increasing the proliferation of these cells in culture (Figure S3M). PC9-BrM3 cells are also metastatic to bone (Nguyen et al., 2009b); neuroserpin overexpression did not markedly affect this activity (Figure 3M,N). Neuroserpin ^{Δ loop} was also ineffective at protecting the parental H2030 and MDA231 cells from apoptosis in brain tissue (Figure 3K,L). These results suggest that neuroserpin mediates brain metastatic activity in cancer cells by inhibiting PA.

Role of anti-PA serpins in brain metastatic breast cancer cells

Unlike the H2030-BrM3 cells, most other brain metastatic models and a large proportion of human brain metastatic tissues overexpressed not one but multiple anti-PA serpins (refer to Figure 1A,I). In MDA231-BrM2, a triple knockdown of the three overexpressed serpins –serpins B2, D1 and neuroserpin– (Figure S4A-C) inhibited the brain metastatic activity of the cells more than did the knockdown of any individual serpin (Figures 4A,B, S4G,H). The knockdown of serpin B2 (Figure S4D,E) partially inhibited the brain metastatic activity of MDA231-BrM2, and the lost activity could be rescued by enforced overexpression of neuroserpin (Figures 4A,B, S4F). We isolated ten clonal cell lines from the MDA231-BrM2 population and determined the expression levels of neuroserpin, serpin B2 and serpin D1 in each cell line. Clonal heterogeneity in serpin expression was evident, with individual clones overexpressing one, two, or all three serpins. Compared to the parental MDA231 population, neuroserpin was upregulated in 9/10 of the clones,

serpin B2 in 5/10 and serpin D1 in 8/10 (Figures 4C, S4I). As a trend, clones overexpressing three serpins were more metastatic to the brain than were clones overexpressing fewer (Figures 4D, S4J). Clones that overexpressed neuroserpin and serpin D1 lost brain metastatic activity when transduced with neuroserpin shRNA (Figure 4E). Serpin B2 was the only upregulated anti-PA serpin in the ErbB2-BrM2 model (refer to Figure 1A). Serpin B2 knockdown in these cells strongly decreased their brain metastatic activity in immunocompetent mice (Figure 4F-H). In sum, the evidence indicated that expression of one or more anti-PA serpins provides lung cancer and breast cancer cells with a critical advantage in the formation of brain metastases.

Metastatic cells face FasL in the brain

We searched plasmin substrate databases (MEROPS, CutDB) for proteins whose cleavage by plasmin might be relevant to brain metastasis. Besides cleaving fibrin in the fibrinolytic cascade, plasmin can cleave certain cytokines, membrane proteins, and extracellular matrix components (Bajou et al., 2008; Chen and Strickland, 1997; Nayeem et al., 1999; Pang et al., 2004). We focused first on FasL as a protein whose cleavage by plasmin might be deleterious to metastatic cells in the brain. FasL is a membrane-anchored homotrimeric protein that binds to the receptor Fas, which activates pro-apoptotic caspases through the adaptor protein FADD (Ashkenazi and Dixit, 1998). FasL is highly expressed in reactive astrocytes in ischemia, brain trauma, Alzheimer's disease, encephalomyelitis and multiple sclerosis (Choi and Benveniste, 2004; Dietrich et al., 2003). Astrocytes are the main source of FasL against invading T cells in experimental encephalomyelitis (Wang et al., 2013). Plasmin cleaves membrane-anchored FasL at Arg144, releasing a soluble pro-apoptotic fragment (sFasL) (Bajou et al., 2008; Fang et al., 2012). Therefore, we tested the hypothesis that anti-PA serpins shield cancer cells from the lethal action of plasmin-mobilized sFasL (Figure 5A).

Immunofluorescence staining of brain sections harboring H2030-BrM3 lesions confirmed that FasL was mainly expressed on reactive astrocytes in the lesions (Figures 5B, S5A). Human and mouse astrocytes also expressed FasL in culture (Figures 5C, S5B). Addition of plasminogen to these cultures decreased the level of cell-associated FasL increasing the cleaved product in the supernatant, as determined by immunostaining and western blotting with antibodies against the extracellular domain of FasL (Figures 5C,D, S5C-E). Mouse brain slices, which contain active plasmin (refer to Figure 2K,

S2O), also contained sFasL. Addition of anti-PA serpins or antiplasmin decreased the level of sFasL in these tissues (Figure 5E). These results suggested a capacity of the PA-plasmin system to mobilize stromal FasL in the brain.

Next we asked whether cancer cells that infiltrate the brain are susceptible to FasL-mediated killing. H2030, PC9, MDA231 and CN34 expressed Fas, as did their BrM derivatives (Figure S5F). Addition of sFasL to BrM cell monolayers caused apoptosis (Figure S5G-I). Addition of sFasL to brain slices harboring H2030-BrM3 (Figure 5F-H), even when α 2-antiplasmin (refer to Figure 2N) was present in the culture (Figure S5J). Conversely, addition of anti-FasL blocking antibody protected parental H2030 cells from apoptosis (Figure 5G-I). Thus, brain metastatic cells are highly susceptible to apoptosis if exposed to FasL in the brain parenchyma.

Neuroserpin shields brain metastatic cells from Fas-mediated killing

To determine whether Fas signaling caused the death of cancer cells that infiltrated the brain, we used a FADD truncation mutant that lacks the death effector domain (FADD-DD construct) and acts as a dominant-negative inhibitor of Fas signaling (Chinnaiyan et al., 1996) (Figure 5J). Transduction of FADD-DD in H2030-BrM3 cell line (Figure 5K) prevented the activation of caspase 3 by sFasL (Figure 5L). The apoptosis that anti-PA serpin-depleted H2030-BrM3 or MDA231-BrM2 cells suffer in brain tissue (refer to Figures 3H-J, S5L) could be prevented by adding anti-FasL blocking antibodies to the tissue culture as well as by enforcing the expression of FADD-DD in the cells (Figures 5M,N, S5L). Moreover, FADD-DD partially rescued the ability of neuroserpin-depleted H2030-BrM3 cells to metastasize in the brain (Figure 5O). Collectively, these results showed that cancer cells that infiltrate the brain succumb to Fas signaling, and anti-PA serpin activity can shield the metastatic cells from FasL attack.

The plasmin target L1CAM mediates cancer cell spreading on brain endothelial cells

Although inhibition of Fas signaling with FADD-DD clearly protected neuroserpin-depleted cancer cells from death in the brain, the metastatic activity of these cells was not fully restored compared to that of wild-type H2030-BrM3 cells (Figure 5O). The neuroserpin-depleted, FADD-DD expressing H2030-BrM3 cells formed smaller lesions that were less well organized alongside capillaries in the brain (Figure S6A). Therefore

we postulated that anti-PA serpins promote brain metastasis by doing more than just preventing FasL action.

Several clues led us to consider L1 cell adhesion molecule (L1CAM) as an additional mediator of brain metastasis downstream of the serpin-PA-plasmin system. L1CAM is mainly expressed in neural tissues and in tumors (Schafer and Altevogt, 2010). It consists of six immunoglobulin-like (Ig) domains, five fibronectin-like (FN) domains, a transmembrane region, and an intracellular domain (Figure 6A). The L1CAM Ig-like repeats mediate homo- and heterophilic interactions for axon guidance during brain development (Maness and Schachner, 2007). L1CAM binds to itself and also to β integrins (Felding-Habermann et al., 1997) and other proteins (Castellani et al., 2002; Donier et al., 2012; Kulahin et al., 2008), and triggers signaling and cytoskeleton remodeling (Herron et al., 2009). Inherited *L1CAM* mutations cause the L1 neurological syndrome (Demyanenko et al., 1999; Maness and Schachner, 2007; Vos and Hofstra, 2010), whereas L1CAM expression in tumors is associated with poor prognosis (Boo et al., 2007; Fogel et al., 2003; Hai et al., 2012; Thies et al., 2002; Tsutsumi et al., 2011; Zhu et al., 2010). Although L1CAM has been implicated in cell invasion (Voura et al., 2001), little is known about its role in cancer. Plasmin cleaves L1CAM at dibasic motifs (Lys860/Lys863), disrupting the capacity for cell-cell adhesion (Nayeem et al., 1999; Silletti et al., 2000) (Figure 6A).

L1CAM was expressed in most parental lines and all the brain metastatic derivatives that we examined, regardless of species or tumor type of origin (Figure S6B,C). We investigated the role of L1CAM as a mediator of heterotypic interactions between H2030-BrM3 cells and monolayers of human brain microvascular endothelial cells (HBMEC) and homotypic interactions with monolayers of H2030-BrM3 cells. H2030-BrM3 cells readily adhered on HBMEC monolayers (Figure 6B). Notably, RNAi-mediated knockdown of L1CAM (Figure S6B) inhibited the ability of H2030-BrM3 cells to bind to HBMEC (Figure 6C) or H2030-BrM3 monolayers (Figure 6D).

Addition of plasmin to monolayers of H2030-BrM3, MDA231-BrM2 and PC9-BrM3 caused a decrease in cell-associated 220kDa L1CAM levels, as shown by anti-L1CAM flow cytometry (Figure 6E) and by the accumulation of a 150kDa L1CAM fragment in the supernatants (Figure 6F) (Mechtersheimer et al., 2001). Moreover, plasmin-treated H2030-BrM3 cells lost capacity to bind to HBMEC monolayers (Figure 6G,H).

L1CAM mediates vascular co-option and metastatic outgrowth

The molecular basis for vascular cooption by cancer cells remains unknown. Given the ability of L1CAM to mediate adhesion of brain metastatic cells to HBMECs, we investigated whether cancer cell L1CAM participates in vascular cooption in the brain. The wild type and the L1CAM-depleted H2030-BrM3 showed a similar proliferation rate in culture (Figure S6D) and a similar ability to infiltrate brain tissue and seek brain capillaries (Figures 6I, S6E). However, L1CAM depletion significantly reduced the ability of H2030-BrM3 and MDA231-BrM2 cells to spread on the abluminal surface of brain capillaries (Figures 6I,J, S6G). Notably, this was accompanied with a marked decrease in the proliferation marker Ki67 in the vessel-associated cancer cells (Figure 6K) but not with changes in apoptosis markers (Figure S6F).

PC9-BrM3 cells do not overexpress endogenous anti-PA serpins. Interestingly, only a small proportion of PC9-BrM3 cells spread on the capillaries in brain slice assays (Figure 6L,M). Enforced expression of neuroserpin in PC9-BrM3 cells, which augments the metastatic activity of these cells (see Figure 3N), significantly increased their spreading on brain capillaries (Figure 6L,M) and their proliferation on the coopted vessels (Figure 6N). Importantly, L1CAM depletion in neuroserpin-overexpressing PC9-BrM3 cells (Figure S6H,I) abrogated the neuroserpin-dependent gains in vascular cooption and cell proliferation (Figure 6L-N). These results showed that L1CAM mediates vascular cooption and outgrowth of metastatic cells in the brain.

L1CAM supports metastasis initiation downstream of neuroserpin

We investigated the role of L1CAM in brain metastasis in vivo. Immunohistochemical analysis of L1CAM of H2030-BrM3 micrometastases showed a localization of this molecule at the interfaces with endothelial cells (identified by nuclei of small, flat morphology and intense H-E staining) and with adjacent cancer cells (Figure 7A). L1CAM knockdown in H2030-BrM3 and MDA231-BrM2 markedly decreased the metastatic activity of these cells in mice (Figure 7B-D). Histologic analysis at day 7 showed that L1CAM-depleted cells did not spread over the capillary network after extravasating in the brain (Figure 7E). Twenty-one days later, these colonies were stalled at the micrometastatic stage (as defined in Figure 3F) (Figure 7F,G). Whereas the wild type cell readily expanded over the capillary network and formed large colonies,

the L1CAM-depleted cells remained mostly as single cells or small clusters that were poorly bound to capillary vessels (Figure 7F,G). Moreover, the gain in metastatic activity imparted by enforced overexpression of neuroserpin in PC9-BrM3 was abrogated by the L1CAM knockdown in these cells (Figure 7H). These results argued that L1CAM expression in metastatic cells acts downstream of neuroserpin to mediate cooption of brain capillaries and metastatic outgrowth.

DISCUSSION

The growing incidence of brain metastasis warrants a better understanding of the molecular mechanisms that underlie this condition. Our findings illuminate two critical requisites for metastatic colonization of the brain, namely, the escape of infiltrating cancer cells from decimation by lethal signals from the reactive stroma, and the striking ability of the surviving cancer cells to coopt brain capillaries during metastatic expansion. We show that a stromal PA-plasmin pathway and its inhibition by carcinoma-derived anti-PA serpins control both of these processes in brain metastasis from lung cancer and breast cancer, suggesting a unified mechanism for metastatic colonization of the brain.

Anti-PA serpins as common mediators of brain metastasis

Brain metastasis involves close and sustained interactions of cancer cells with brain capillaries and reactive astrocytes. Previous work (Kienast et al., 2010; Lorgier and Felding-Habermann, 2010) and our own data show that circulating cancer cells in brain capillaries interact with the BBB endothelium not only during extravasation but subsequently as well, by attaching to the abluminal surface for metastatic outgrowth as a furrow along the coopted vessels. The cancer cells are also immediately exposed to astrocytes, which are present in the perivascular space and contact the endothelium to form the BBB (Abbott et al., 2006). We show that astrocytes act as a source of deleterious signals to repel invading cells. Astrocytes may eventually support the growth of brain metastasis by providing growth factors (Seike et al., 2011) and GAP junctions (Lin, 2010). However, in order to benefit from these trophic inputs, cancer cells must first avert the deleterious effects of the reactive stroma.

Expression of anti-PA serpins in the cancer cells provides such a shield. We show that brain metastatic lung and breast cancer cells from human or murine origins express high levels of anti-PA serpins compared to counterparts that are lowly metastatic to the brain. Three out of four known anti-PA serpins, and serpin D1 are expressed in the six experimental models that we investigated. The most prominent anti-PA serpins in these models, neuroserpin and serpin B2, are also expressed in a majority of the human brain metastasis samples from lung cancer and breast cancer patients that we examined. In functional assays these serpins and their PA inhibitory activity are limiting for metastatic colonization of the brain.

The PA-plasmin system is well characterized in connection with its role in blood clot resolution. In cancer however the PA-plasmin system is paradoxically implicated both in tumor suppression and tumor progression. Plasmin is thought to promote cancer cell proliferation and invasion by cleaving growth factor precursors and extracellular matrix components (McMahon and Kwaan, 2008). However, the anti-PA serpin E1 in tumors and in blood is associated with poor clinical outcome in lung, breast, and gastrointestinal cancers (Allgayer et al., 1997; Berger, 2002; Foekens et al., 1995; Harbeck et al., 1999). The same holds for serpin B2 in lung cancer (Morita et al., 1998). The role of PA and plasmin in tumor progression therefore has remained obscure. Here we show that anti-PA serpins shield metastatic cells from PA-plasmin in the brain, with a clear pro-metastatic advantage.

Shielding cancer cells from Fas death signals in the brain

Our results suggest that the PA-plasmin system acting through FasL creates a highly hostile environment for infiltrating cancer cells in the brain. Although FasL plays important roles in immune homeostasis (Krammer, 2000) and is present in tumors (Baldini et al., 2009) its expression is particularly acute in reactive astrocytes (Beer et al., 2000). Astrocytes are the main source of FasL in response to infiltrating leukocytes, and of PAs in response to brain injury (Adhami et al., 2008; Bechmann et al., 2002; Ganesh and Chintala, 2011; Teesalu et al., 2001). Astrocyte-derived FasL plays a central role in repelling invading autoimmune T cells in the brain (Wang et al., 2013). We observed that metastasis-associated astrocytes express both PA and FasL, that plasmin releases membrane-bound FasL from astrocytes, and that sFasL levels in brain tissue depend on plasmin. Addition of anti-PA serpins, anti-plasmin serpins, or FasL-blocking antibodies to brain tissue protects infiltrating cancer cells. Moreover, brain metastatic cells from lung or breast cancers are highly sensitive to sFasL-induced apoptosis, and suffer Fas-dependent death in the brain unless they express anti-PA serpins. We conclude that the attrition of infiltrating cancer cells in the brain is mediated by Fas signaling and impeded by anti-PA serpins. Cancer cells that express anti-PA serpins therefore have a strong advantage in the PA-rich microenvironment of the brain.

L1CAM-mediated vascular cooption for metastatic outgrowth

Avoiding FasL-mediated death is not the only pro-metastatic benefit provided by anti-PA serpins. We show that neuroserpin additionally promotes vascular cooption –the spreading of the cancer cells on the vasculature. This effect depends on expression of the plasmin-labile molecule L1CAM in cancer cells. L1CAM expression is normally restricted to neurons where it mediates axonal guidance through interactions of the growth cone with surrounding components (Castellani et al., 2002; Wiencken-Barger et al., 2004). We show that L1CAM expression in cancer cells mediates their adhesion and spreading on brain endothelial cells in culture and on capillaries in the brain. L1CAM additionally mediates interactions between cancer cells. Plasmin cleaves L1CAM inactivating these binding activities. When depleted of L1CAM, brain metastatic cells fail to coopt brain capillaries, and metastatic outgrowth stalls. The evidence suggests that neuroserpin prevents plasmin-mediated destruction of L1CAM in brain metastatic cells, fostering vascular cooption by these cells and further enhancing metastasis.

The finding that L1CAM is a mediator of cancer cell spreading on capillaries provides unexpected insights into the molecular basis for vascular cooption in cancer. A striking feature of brain metastasis is the ability of metastatic cells to remain closely attached to the capillary network after extravasation (Kienast et al., 2010; Lörger and Felding-Habermann, 2010). Vascular cooption is thought to be important for brain metastasis (Carbonell et al., 2009) and for cancer cell escape from therapy-induced hypoxia (Leenders et al., 2004). Despite the likely importance of vascular cooption in cancer, the molecular basis of this process is unknown. The present identification of L1CAM as a mediator of metastatic vascular cooption provides an opening for the mechanistic and functional dissection of this process.

Implications beyond brain metastasis

The molecular mechanisms identified here protect metastatic cells from selective pressures that are particularly acute in the brain but may also be relevant in other contexts. The high mortality of cancer cells that infiltrate distant organs is characteristic of metastasis in general (Gupta and Massagué, 2006; Valastyan and Weinberg, 2011), and vascular cooption has been observed in metastasis to other organs and by other types of cancer (Blouw et al., 2003; Leenders et al., 2002; Leenders et al., 2004). The brain microenvironment can certainly select for brain-specific metastatic traits in cancer cells (Bos et al., 2009; Nguyen et al., 2009b). However, evading death signals and

interacting with the vasculature are basic needs of metastatic cells in all organs, not only in the brain. We note that the serpins overexpressed in our brain metastatic models are also expressed, albeit at lower levels, in counterparts that are metastatic to other organs (refer to **Figure 1B**). Moreover, L1CAM expression in primary tumors is associated with poor prognosis in various types of cancer (Boo et al., 2007; Doberstein et al., 2011; Fogel et al., 2003; Schroder et al., 2009; Thies et al., 2002; Tischler et al., 2011; Tsutsumi et al., 2011). PA, plasmin, and FasL have also been implicated in disease progression in other cancers (McMahon and Kwaan, 2008; Timmer et al., 2002).

The reactive brain stroma and its high capacity to generate PA-plasmin and FasL may be more challenging to infiltrating cancer cells than is the stroma in other organs. As a result, the brain may select for more accentuated versions of otherwise general metastatic traits. Although anti-PA serpins, plasmin, FasL and L1CAM had not been previously connected in a unified mechanism or linked to metastatic cell survival and vascular cooption, their repeated clinical association with poor prognosis may reflect a wider role in metastasis than we have demonstrated here. The present insights into what decimates invading cancer cells in the brain, and how these cells shield themselves from stromal attack could be leveraged for the prevention and treatment of metastasis in the brain and perhaps in other organs as well.

Acknowledgments

We would like to thank A. Boire, P. Bos, L. DeAngelis, E. Holland and J. Posner for helpful input, the Brain Tumor Center for tumor samples, Marija Drobnjak for establishing tissue microarray from lung cancer brain metastasis, T. Jacks for cell lines and A. Thorburn for reagents. This work was supported by NIH grants P01-CA129243 and U54-163167, DOD Innovator award W81XWH-12-0074, and the Alan and Sandra Gerry Metastasis Research Initiative (J.M.). M.V. is a Hope Funds for Cancer Research postdoctoral fellow. A.C.O. is an Erwin Schrödinger Fellowship awardee (J3013, FWF, Austrian Science Fund). X.Z. is a McNair Scholar and the recipient of a grant from Breast Cancer Research Foundation. J.M. is an investigator of the Howard Hughes Medical Institute.

EXPERIMENTAL PROCEDURES

Brain metastatic cell isolation and culture. Human brain metastatic cell lines were previously described (Bos et al., 2009; Nguyen et al., 2009b). A ErbB2-P cell line was established from MMTV driven-NeuNT transgenic mammary tumors in mice (Muller et al., 1988). ErbB2-P cells were injected intracardiacally to obtain brain metastatic derivatives. Briefly, a cell suspension containing 10^5 ErbB2-P cells expressing a TK-GFP-Luciferase (TGL) construct, in a volume of 100 μ l was injected in the left cardiac ventricle of anesthetized 4–6 week-old FVB/NCr mice. Tumor development was monitored by weekly bioluminescence imaging using the IVIS-200 imaging system from Xenogen as previously described. Brain lesions were localized by *ex vivo* bioluminescence imaging, and resected under sterile conditions. Tissue was minced and placed in culture medium containing a 1:1 mixture of DMEM/Ham's F12 supplemented with 0.125% collagenase III and 0.1% hyaluronidase. Samples were incubated at room temperature for 4–5 h, with gentle rocking. After collagenase treatment, cells were briefly centrifuged, resuspended in 0.25% trypsin, and incubated for a further 15 min in a 37 °C water bath. Cells were resuspended in culture media and allowed to grow to confluence on a 10cm dish. GFP+ cells were sorted for further propagation in culture or inoculation in mice

MDA231-BrM2, ErbB2-BrM2, 373N1, 393N1, 482N1, 2691N1 were cultured in DME media supplemented with 10% fetal bovine serum (FBS), 2mM L-Glutamine, 100IU/ml penicillin/streptomycin and 1 μ g/ml amphotericin B. CN34-BrM2 were cultured in M199 media supplemented with 2.5% fetal bovine serum (FBS), 10 μ g/ml insulin, 0.5 μ g/ml hydrocortisone, 20ng/ml EGF, 100ng/ml cholera toxin, 1 μ g/ml amphotericin B, and 100 U/ml penicillin/streptomycin. H2030-BrM3 and PC9-BrM3 were cultured in RPMI1640 media supplemented with 10% fetal bovine serum (FBS), 2mM L-Glutamine, 100IU/ml penicillin/streptomycin, and 1 μ g/ml amphotericin B. For retrovirus and lentivirus production, GPG29 and 293T cells, respectively, were cultured in DME media supplemented with 10% fetal bovine serum (FBS), 2mM L-Glutamine, 100IU/ml penicillin/streptomycin, and 1 μ g/ml amphotericin B. In addition the GPG29 media contained 0.3mg/ml G418, 20ng/ml doxycycline and 2 μ g/ml puromycin. MDA231-BrM2 SCP were prepared by serial dilution as previously shown (Kang et al., 2003) and cultured in DME media supplemented with 10% fetal bovine serum (FBS), 2mM L-Glutamine, 100IU/ml penicillin/streptomycin, and 1 μ g/ml amphotericin B. Mouse

microglia cells were acquired at ATCC (CRL-2467). Mouse astrocytes were obtained from two-day old pups (Schildge et al., 2013). In brief, brains were mechanically dissociated, filtered through 100 μ m filters and cell suspension cultured in a petri dish under normal conditions during the next 10 days. On day 10, the dish was incubated overnight at 37°C with gentle shaking. Next day media was changed and astrocyte enrichment confirmed with >90% of cells staining positive for GFAP.

Animal studies. All experiments using animals were done in accordance to a protocol approved by MSKCC Institutional Animal Care and Use Committee (IACUC). Athymic NCR nu/nu (NCI-Frederick), Cr:NIH bg-nu-xid (NCI-Frederick), FVB/NCr (NCI-Frederick), and B6129SF1/J (Jackson Laboratory) female mice aged between 4-6 weeks were used for animal experiments. Brain colonization assays were performed as described previously (Bos et al., 2009; Nguyen et al., 2009b). Briefly, 50,000 (for long term experiments) or 500,000 (for short term experiments) of MDA231-BrM2a, CN34BrM-2c, H2030-BrM3, PC9-BrM3 and 100,000 for syngeneic cell lines 373N1, 393N1, 482N1, 2691N1, ErbB2-BrM2 cells resuspended in 100 μ l of PBS and injected in the left ventricle. Brain colonization was analyzed in-vivo and ex-vivo by bioluminescence imaging (BLI). Anesthetized mice (ketamine 100mg/kg/xylazine 10mg/kg) were injected retro-orbitally with D-Luciferin (150mg/kg) and imaged with an IVIS Spectrum Xenogen machine (Caliper Life Sciences). Bioluminescence analysis was performed using Living Image software, version 2.50.

Gene expression analysis. Whole RNA was isolated from cells using RNAeasy Mini Kit (Qiagen). 1000ng RNA was used to generate cDNA using Transcriptor First Strand cDNA synthesis kit (Roche). Gene expression was analyzed using Taqman gene expression assays (Applied Biosystems). Assays used for human genes: *FADD* (Hs04187499_m1), *FASL* (Hs00181225_m1), *L1CAM* (Hs01109748_m1), *SERPINB2* (Hs00234032_m1), *SERPIND1* (Hs00164821_m1), *SERPINE1* (Hs01126604_m1), *SERPINE2* (Hs00385730_m1), *SERPINI1* probe#1 (Hs01115397_m1), *SERPINI1* probe#2 (Hs01115400_m1). Assays used for the mouse genes: *fasL* (Mm00438864_m1), *serpinb2* (Mm00440905_m1), *serpind1* (Mm00433939_m1), *serpine2* (Mm00436753_m1), *serpin1* (Mm00436740_m1). Relative gene expression was normalized to the “housekeeping” genes namely β 2M (Hs99999907_m1) and β 2m (Mm00437762_m1). Quantitative PCR reaction was performed on ABI 7900HT Fast Real-Time PCR system and analyzed using the software SDS2.2.2 (Applied

Biosystems).

Clinical samples and immunohistochemistry. Thirty-three and 123 cases from lung and breast cancer brain metastasis respectively were obtained from the Brain Tumor Center and the Department of Pathology at MSKCC. Paraffin embedded tissue microarrays from brain metastases obtained from breast and lung cancer were obtained from the MSKCC Department of Pathology in compliance with protocols approved by the MSKCC Institutional Review Board (IRB). Immunohistochemistry for Neuroserpin (Abcam, ab16171-100, Lot number 158358, 1:250) and SerpinB2 (Santa Cruz, sc-25745, Lot number L1406, 5 µg/ml) were performed by the MSKCC Molecular Cytology Core Facility using standardized automated protocols. Immunoreactivity stainings were evaluated and scored by clinical pathologists (J.T.H., E.B.) in a blinded fashion. 42 brain metastasis samples from breast cancer were annotated for the primary tumor type, corresponding to 27 cases positive for neuroserpin and 12 for serpin B2. Analysis of expression of *SERPINB2* and *SERPINI1* was performed by using the MSKCC dataset #1 (Nguyen et al., 2009b), including 107 samples of which 106 had clinical information available. The hazard ratio of the average value of *SERPINI1* and *SERPINB2* was computed based on Cox Proportional Hazards Models, as implemented by the “coxph” command in R.

Brain slice assays. Organotypic slice cultures from adult mouse brain were prepared adapting previously described methods (Polleux and Ghosh, 2002). Brains (4-6 week old athymic NCR nu/nu mice) were dissected in Hank's Balanced Salt Solution (HBSS) supplemented with HEPES (pH 7.4) (2.5mM), D-glucose (30mM), CaCl₂ (1mM), MgSO₄ (1mM), NaHCO₃ (4mM), and were embedded in low-melting agarose (Lonza) pre-heated at 42° C. The embedded brains cut into 250µm slices using a vibratome (Leica). Brain slices (bregma -1mm to +3mm) were placed with flat spatulas on top of 0.8µm pore membranes (Millipore) in slice culture media (DMEM, supplemented HBSS, FBS 5%, L-Glutamine (1mM), 100IU/mL penicillin, 100µg/mL streptomycin). Brain slices were incubated at 37°C and 5% CO₂ for 1 h, and then 3x10⁴ cancer cells suspended in 2 µL of culture media were placed on the surface of the slice and incubated for 48-72 hours. Brain slices could be maintained under these conditions for up to five days without apparent alterations in tissue architecture. α2-antiplasmin (Molecular Innovations, 2.5µg/ml), neuroserpin and serpin B2 (Peprotech, 0.5µg/ml each) were added to the medium. sFasL (Peprotech, 500ng/ml) or FasL blocking antibodies (BD, 12.5µg/ml) were

added to the medium, and slices pre-incubated for 24 hours before addition of cancer cells. Brain slices were fixed in PFA 4%, overnight and then free-floating immunofluorescence performed for GFP (Aves lab, ref. GFP-1020, 1:1000), cleaved caspase-3 (Cell Signaling, ref. 9661, 1:500), collagen IV (Millipore, ref. AB756P, 1:500). Nuclei were stained with Bis-Benzamide (SIGMA, 1µg/ml). Slices were mounted with ProLong Gold anti fade reagent (Invitrogen).

Plasmids, recombinant proteins and in vitro experiments. Human Neuroserpin cDNA (Open Biosystems) was subcloned into the pBABE-puro retroviral expression vector. Site directed mutagenesis (Stratagene) was performed to generate the Δ loop mutant previously characterized (Takehara et al., 2009). TRC number for shRNAs used in this study are Neuroserpin (TRCN0000052356 and TRCN0000052355), SERPINB2 (TRCN0000052278), SERPIND1 (TRCN 0000052226), SERPINE2 (TRCN 0000052317), L1CAM (TRCN0000063916). All shRNAs were specific against the human gene and expressed in pLKO.1-shRNA vectors (Open Biosystems) with Puromycin, Hygromycin or Neomycin (G418) resistance genes. The *ST6Gal/NaC5* shRNA was previously described (Bos et al., 2009). The FADD-DD construct was kindly provided by Andrew M. Thornburn and subcloned in a pLVX-hygro lentiviral expression vector. Neuroserpin ELISA was performed following manufacturer's instructions (Peprotech). DVL-K chromogenic assays were performed by plating 5×10^4 cells in 24 well plates and starvation in DMEM FBS 0.25% overnight. Plasminogen (Molecular innovations, 0.125µM) was added to cancer cells that were incubated for 24 hours prior to DVL-K chromogenic assays. D-VLK chromogenic substrate (Molecular Innovations) was prepared following manufacturer's instructions. D-VLK was added to cells and a change in absorbance was monitored at 405 nm. For (3-(4,5-dimethylthiazolyl-2-yl)-2,5-diphenyltetrazolium bromide (MTT) cell proliferation assays, 5×10^2 cells were plated in 96 well plates, and for cleaved Caspase-3, 25×10^3 cells were plated in 24 well plates, starved with FBS 0.25% overnight in presence or absence of sFasL (Peprotech, 100-500ng/ml) and incubated for the indicated period of time. Plasmin (Molecular Innovations) treatment of cells was done at 1.6U/ml for 4 hours.

Immunofluorescence. Tissue for immunofluorescence was obtained after overnight fixation with PFA 4% at 4°C. Slicing of the brain was done by using a vibratome (Leica) or sliding microtome (Fisher). Both types of brain slices (250µm and 80µm respectively) were blocked in NGS 10%, BSA 2%, Triton 0.25% in PBS for 2 hours at room

temperature (RT). Primary antibodies were incubated overnight at 4C in the blocking solution and the following day for 30 minutes at RT. After extensive washing in PBS-Triton 0.25%, the secondary antibody was added in the blocking solution and incubated for 2 hours. After extensive washing in PBS-Triton 0.25%, nuclei were stained with Bis-Benzamide for 7 minutes at RT. Primary antibodies: GFP (Aves Labs, ref. GFP-1020, 1:1000), Plasminogen (Santa Cruz, ref. sc-25546, 1:100), tPA (Molecular Innovations, ref. ASMPA-GF, 1:50), uPA (Molecular Innovations, ref. ASMUPA-GF, 1:50), GFAP (Dako, ref. Z0334, and Millipore, ref. MAB360, both 1:1000), Ibal (Wako, ref. 019-19741, 1:500), Col.IV (Millipore, ref. AB756P, 1:500), NeuN (Millipore, ref. MAB377, 1:500), Neuroserpin (Abcam, ref. ab16171, 1:250), FasL (Santa Cruz, ref. sc-834 and sc-6237, 1:100), L1CAM (Millipore, ref. CBL275, 1:200 and Covance, ref. SIG-3911, 1µg/ml). Secondary antibodies: Alexa-Fluor anti-chicken⁴⁸⁸, anti-rabbit⁵⁵⁵, anti-mouse⁵⁵⁵, anti-mouse⁶³³ (Invitrogen).

Immunoblotting. Cell pellets were lysed with RIPA buffer and protein concentrations were determined by BSA Protein Assay Kit (Pierce). Proteins were separated by SDS-PAGE and transferred to nitrocellulose membranes or PVDF membranes. Membranes were immunoblotted with antibodies against FAS (Santa Cruz, ref. sc-715, 1:100), FasL (Santa Cruz, ref. sc-834 and sc-6237 1:100), L1CAM (Millipore, ref. CBL275, eBioscience, ref. 14-1719, and Abcam, ref. ab24345, 1: 200-1000), FLAG (Sigma, 1:2000), Serpin B2 (Abcam, ref. 47742, 1:500), Tubulin (Cell signaling, 1:2000).

Confocal microscopy and image analysis. Images were acquired with a Leica SP5 up-right confocal microscope 10X, 20X, 40X and 63X objectives and images were analyzed with ImageJ, Imaris and Metamorph softwares. In brain slice assays, GFP+ cell bodies that were located >40µm from the surface of the slice were considered for analysis in order to avoid cells clusters remaining on the surface. ImageJ was used to determine the spread cell index by using confocal images and applying the round filter with a 0.45 threshold.

In vitro blood–brain barrier assay. This assay was performed as previously described (Bos et al., 2009). Briefly, primary human umbilical vein endothelial cells (HUVEC, ScienCell) were co-cultured with human primary astrocytes (ScienCell), on opposite sides of a polylysine-treated, gelatin-coated tissue culture transwell insert for 3 days. In brief, 3µm pore PET tissue culture inserts (Fisher) were treated with polylysine (1µg/ml,

Millipore) overnight, washed four times, and coated with 0.2% gelatin (Sigma) for a minimum of 30 min. Inserts were placed upside-down in a 15 cm plate, and 10^5 primary human astrocytes were plated on the membrane surface. Astrocytes were fed every 15 min for 5 h, and the inserts were then flipped and placed in 24-well plates. 5×10^5 endothelial cells were plated on the upper chamber of the inserts, and cultures were placed in the incubator, without further perturbation. For BBB transmigration assays, 5×10^5 cells were seeded on the upper chamber and incubated for 14–18 h. Inserts were washed with PBS and fixed with 4% PFA for 20 min. The membranes were removed from the plastic insert, immunofluorescence against GFP was performed and mounted on a microscope slide. Pictures of multiple fields from 5–8 inserts per experiment were taken, and the number of transmigrated cells was counted.

Flow cytometry. Monolayers of adherent cells were detached using 1mM EDTA, resuspended in single cell suspensions and incubated with fluorochrome-conjugated monoclonal antibodies of human L1CAM (eBioscience, ref. 12-1719-42). The cell surface expression of L1CAM was analyzed by a FACSCalibur flow cytometer (BD Biosciences).

Cell adhesion assays. HBMEC or tumor cells were plated in 2-well culture slides (BD Falcon) and allowed to grow over 90% confluent. Tumor cells were labeled with CellTracker™ Green CMFDA (5-Chloromethylfluorescein Diacetate) (Molecular Probes). 7.2×10^4 pre-labeled tumor cells were allowed to adhere to the monolayer of cancer cells for 20 min. After washing off the non-adherent cells, the slides were fixed with 1% paraformaldehyde and mounted with mounting medium with DAPI (Vector Labs). Adherent cells (green) and the nucleus of total cells (blue) were scored by fluorescence microscopy. The number of GFP+ cancer cells adhered to HBMEC or cancer cells covering the bottom of every well was calculated.

REFERENCES

- Abbott, N.J., Ronnback, L., and Hansson, E. (2006). Astrocyte-endothelial interactions at the blood-brain barrier. *Nat Rev Neurosci* 7, 41-53.
- Adhami, F., Yu, D., Yin, W., Schloemer, A., Burns, K.A., Liao, G., Degen, J.L., Chen, J., and Kuan, C.Y. (2008). Deleterious effects of plasminogen activators in neonatal cerebral hypoxia-ischemia. *Am J Pathol* 172, 1704-1716.
- Allgayer, H., Heiss, M.M., and Schildberg, F.W. (1997). Prognostic factors in gastric cancer. *Br J Surg* 84, 1651-1664.
- Ashkenazi, A., and Dixit, V.M. (1998). Death receptors: signaling and modulation. *Science* 281, 1305-1308.
- Bai, H., Baik, N., Kiosses, W.B., Krajewski, S., Miles, L.A., and Parmer, R.J. (2011). The novel plasminogen receptor, plasminogen receptor(KT) (Plg-R(KT)), regulates catecholamine release. *J Biol Chem* 286, 33125-33133.
- Bajou, K., Peng, H., Laug, W.E., Maillard, C., Noel, A., Foidart, J.M., Martial, J.A., and DeClerck, Y.A. (2008). Plasminogen activator inhibitor-1 protects endothelial cells from FasL-mediated apoptosis. *Cancer Cell* 14, 324-334.
- Baldini, E., Ulisse, S., Marchioni, E., Di Benedetto, A., Giovannetti, G., Petrangeli, E., Sentinelli, S., Donnorso, R.P., Reale, M.G., Mottolese, M., *et al.* (2009). Expression of Fas and Fas ligand in human testicular germ cell tumours. *Int J Androl* 32, 123-130.
- Barnholtz-Sloan, J.S., Sloan, A.E., Davis, F.G., Vigneau, F.D., Lai, P., and Sawaya, R.E. (2004). Incidence proportions of brain metastases in patients diagnosed (1973 to 2001) in the Metropolitan Detroit Cancer Surveillance System. *J Clin Oncol* 22, 2865-2872.
- Bechmann, I., Steiner, B., Gimsa, U., Mor, G., Wolf, S., Beyer, M., Nitsch, R., and Zipp, F. (2002). Astrocyte-induced T cell elimination is CD95 ligand dependent. *J Neuroimmunol* 132, 60-65.
- Beer, R., Franz, G., Schopf, M., Reindl, M., Zelger, B., Schmutzhard, E., Poewe, W., and Kampfl, A. (2000). Expression of Fas and Fas ligand after experimental traumatic brain injury in the rat. *J Cereb Blood Flow Metab* 20, 669-677.
- Benarroch, E.E. (2007). Tissue plasminogen activator: beyond thrombolysis. *Neurology* 69, 799-802.
- Berger, D.H. (2002). Plasmin/plasminogen system in colorectal cancer. *World J Surg* 26, 767-771.
- Blouw, B., Song, H., Tihan, T., Bosze, J., Ferrara, N., Gerber, H.P., Johnson, R.S., and Bergers, G. (2003). The hypoxic response of tumors is dependent on their microenvironment. *Cancer Cell* 4, 133-146.
- Boo, Y.J., Park, J.M., Kim, J., Chae, Y.S., Min, B.W., Um, J.W., and Moon, H.Y. (2007). L1 expression as a marker for poor prognosis, tumor progression, and short survival in patients with colorectal cancer. *Ann Surg Oncol* 14, 1703-1711.
- Bos, P.D., Zhang, X.H., Nadal, C., Shu, W., Gomis, R.R., Nguyen, D.X., Minn, A.J., van de Vijver, M.J., Gerald, W.L., Foekens, J.A., *et al.* (2009). Genes that mediate breast cancer metastasis to the brain. *Nature* 459, 1005-1009.
- Carbonell, W.S., Ansoorge, O., Sibson, N., and Muschel, R. (2009). The vascular basement membrane as "soil" in brain metastasis. *PLoS one* 4, e5857.
- Castellani, V., De Angelis, E., Kenwrick, S., and Rougon, G. (2002). Cis and trans interactions of L1 with neuropilin-1 control axonal responses to semaphorin 3A. *EMBO J* 21, 6348-6357.
- Chambers, A.F., Groom, A.C., and MacDonald, I.C. (2002). Dissemination and growth of cancer cells in metastatic sites. *Nat Rev Cancer* 2, 563-572.

- Chambers, A.M., I; Schmidt, E; Morris, V; Groom, A (2000). Clinical targets for anti-metastasis therapy. *Adv Cancer Res* 79, 91-121.
- Chen, Z.L., and Strickland, S. (1997). Neuronal death in the hippocampus is promoted by plasmin-catalyzed degradation of laminin. *Cell* 91, 917-925.
- Chinnaiyan, A.M., Tepper, C.G., Seldin, M.F., O'Rourke, K., Kischkel, F.C., Hellbardt, S., Krammer, P.H., Peter, M.E., and Dixit, V.M. (1996). FADD/MORT1 is a common mediator of CD95 (Fas/APO-1) and tumor necrosis factor receptor-induced apoptosis. *J Biol Chem* 271, 4961-4965.
- Choi, C., and Benveniste, E.N. (2004). Fas ligand/Fas system in the brain: regulator of immune and apoptotic responses. *Brain Res Rev* 44, 65-81.
- Demyanenko, G.P., Tsai, A.Y., and Maness, P.F. (1999). Abnormalities in neuronal process extension, hippocampal development, and the ventricular system of L1 knockout mice. *J Neurosci* 19, 4907-4920.
- Dietrich, P.Y., Walker, P.R., and Saas, P. (2003). Death receptors on reactive astrocytes: a key role in the fine tuning of brain inflammation? *Neurology* 60, 548-554.
- Doberstein, K., Wieland, A., Lee, S.B., Blaheta, R.A., Wedel, S., Moch, H., Schraml, P., Pfeilschifter, J., Kristiansen, G., and Gutwein, P. (2011). L1-CAM expression in ccRCC correlates with shorter patients survival times and confers chemoresistance in renal cell carcinoma cells. *Carcinogenesis* 32, 262-270.
- Donier, E., Gomez-Sanchez, J.A., Grijota-Martinez, C., Lakoma, J., Baars, S., Garcia-Alonso, L., and Cabedo, H. (2012). L1CAM binds ErbB receptors through Ig-like domains coupling cell adhesion and neuregulin signalling. *PLoS one* 7, e40674.
- Fabbro, S., and Seeds, N.W. (2009). Plasminogen activator activity is inhibited while neuroserpin is up-regulated in the Alzheimer disease brain. *J Neurochem* 109, 303-315.
- Fang, H., Placencio, V.R., and DeClerck, Y.A. (2012). Protumorigenic activity of plasminogen activator inhibitor-1 through an antiapoptotic function. *J Natl Cancer Inst* 104, 1470-1484.
- Feld, R., Rubinstein, L.V., and Weisenberger, T.H. (1984). Sites of recurrence in resected stage I non-small-cell lung cancer: a guide for future studies. *J Clin Oncol* 2, 1352-1358.
- Felding-Habermann, B., Silletti, S., Mei, F., Siu, C.H., Yip, P.M., Brooks, P.C., Cheresh, D.A., O'Toole, T.E., Ginsberg, M.H., and Montgomery, A.M. (1997). A single immunoglobulin-like domain of the human neural cell adhesion molecule L1 supports adhesion by multiple vascular and platelet integrins. *J Cell Biol* 139, 1567-1581.
- Fidler, I.J. (2003). The pathogenesis of cancer metastasis: the 'seed and soil' hypothesis revisited. *Nat Rev Cancer* 3, 453-458.
- Foekens, J.A., Look, M.P., Peters, H.A., van Putten, W.L., Portengen, H., and Klijn, J.G. (1995). Urokinase-type plasminogen activator and its inhibitor PAI-1: predictors of poor response to tamoxifen therapy in recurrent breast cancer. *J Natl Cancer Inst* 87, 751-756.
- Fogel, M., Gutwein, P., Mechttersheimer, S., Riedle, S., Stoeck, A., Smirnov, A., Edler, L., Ben-Arie, A., Huszar, M., and Altevogt, P. (2003). L1 expression as a predictor of progression and survival in patients with uterine and ovarian carcinomas. *Lancet* 362, 869-875.
- Francia, G., Cruz-Munoz, W., Man, S., Xu, P., and Kerbel, R.S. (2011). Mouse models of advanced spontaneous metastasis for experimental therapeutics. *Nat Rev Cancer* 11, 135-141.
- Fujimoto, S., Katsuki, H., Ohnishi, M., Takagi, M., Kume, T., and Akaike, A. (2008). Plasminogen potentiates thrombin cytotoxicity and contributes to pathology of intracerebral hemorrhage in rats. *J Cereb Blood Flow Metab* 28, 506-515.

- Ganesh, B.S., and Chintala, S.K. (2011). Inhibition of reactive gliosis attenuates excitotoxicity-mediated death of retinal ganglion cells. *PLoS one* 6, e18305.
- Gavrilovic, I.T., and Posner, J.B. (2005). Brain metastases: epidemiology and pathophysiology. *J Neurooncol* 75, 5-14.
- Gupta, G.P., and Massagué, J. (2006). Cancer metastasis: building a framework. *Cell* 127, 679-695.
- Gutierrez-Fernandez, A., Gingles, N.A., Bai, H., Castellino, F.J., Parmer, R.J., and Miles, L.A. (2009). Plasminogen enhances neuritegenesis on laminin-1. *J Neurosci* 29, 12393-12400.
- Hai, J., Zhu, C.Q., Bandarchi, B., Wang, Y.H., Navab, R., Shepherd, F.A., Jurisica, I., and Tsao, M.S. (2012). L1 cell adhesion molecule promotes tumorigenicity and metastatic potential in non-small cell lung cancer. *Clin Cancer Res* 18, 1914-1924.
- Harbeck, N., Thomssen, C., Berger, U., Ulm, K., Kates, R.E., Hofler, H., Janicke, F., Graeff, H., and Schmitt, M. (1999). Invasion marker PAI-1 remains a strong prognostic factor after long-term follow-up both for primary breast cancer and following first relapse. *Breast Cancer Res Treat* 54, 147-157.
- Herron, L.R., Hill, M., Davey, F., and Gunn-Moore, F.J. (2009). The intracellular interactions of the L1 family of cell adhesion molecules. *Biochem J* 419, 519-531.
- Heyn, C., Ronald, J.A., Ramadan, S.S., Snir, J.A., Barry, A.M., MacKenzie, L.T., Mikulis, D.J., Palmieri, D., Bronder, J.L., Steeg, P.S., *et al.* (2006). In vivo MRI of cancer cell fate at the single-cell level in a mouse model of breast cancer metastasis to the brain. *Magn Reson Med* 56, 1001-1010.
- Hoover-Plow, J., Skomorovska-Prokvolit, O., and Welsh, S. (2001). Selective behaviors altered in plasminogen-deficient mice are reconstituted with intracerebroventricular injection of plasminogen. *Brain Res* 898, 256-264.
- Irving, J.A., Pike, R.N., Lesk, A.M., and Whisstock, J.C. (2000). Phylogeny of the serpin superfamily: implications of patterns of amino acid conservation for structure and function. *Genome Res* 10, 1845-1864.
- Kang, Y., Siegel, P.M., Shu, W., Drobnjak, M., Kakonen, S.M., Cordon-Cardo, C., Guise, T.A., and Massagué, J. (2003). A multigenic program mediating breast cancer metastasis to bone. *Cancer Cell* 3, 537-549.
- Karrison, T.G., Ferguson, D.J., and Meier, P. (1999). Dormancy of mammary carcinoma after mastectomy. *J Natl Cancer Inst* 91, 80-85.
- Kienast, Y., von Baumgarten, L., Fuhrmann, M., Klinkert, W.E., Goldbrunner, R., Herms, J., and Winkler, F. (2010). Real-time imaging reveals the single steps of brain metastasis formation. *Nat Med* 16, 116-122.
- Kim, S.J., Kim, J.S., Park, E.S., Lee, J.S., Lin, Q., Langley, R.R., Maya, M., He, J., Kim, S.W., Weihua, Z., *et al.* (2011). Astrocytes upregulate survival genes in tumor cells and induce protection from chemotherapy. *Neoplasia* 13, 286-298.
- Krammer, P.H. (2000). CD95's deadly mission in the immune system. *Nature* 407, 789-795.
- Kulahin, N., Li, S., Hinsby, A., Kiselyov, V., Berezin, V., and Bock, E. (2008). Fibronectin type III (FN3) modules of the neuronal cell adhesion molecule L1 interact directly with the fibroblast growth factor (FGF) receptor. *Mol Cell Neurosci* 37, 528-536.
- Law, R.H., Zhang, Q., McGowan, S., Buckle, A.M., Silverman, G.A., Wong, W., Rosado, C.J., Langendorf, C.G., Pike, R.N., Bird, P.I., *et al.* (2006). An overview of the serpin superfamily. *Genome Biol* 7, 216.
- Leenders, W.P., Kusters, B., and de Waal, R.M. (2002). Vessel co-option: how tumors obtain blood supply in the absence of sprouting angiogenesis. *Endothelium* 9, 83-87.
- Leenders, W.P., Kusters, B., Verrijp, K., Maass, C., Wesseling, P., Heerschap, A., Ruiter, D., Ryan, A., and de Waal, R. (2004). Antiangiogenic therapy of cerebral

melanoma metastases results in sustained tumor progression via vessel co-option. *Clin Cancer Res* 10, 6222-6230.

Leyland-Jones, B. (2009). Human epidermal growth factor receptor 2-positive breast cancer and central nervous system metastases. *J Clin Oncol* 27, 5278-5286.

Li, B., Wang, C., Zhang, Y., Zhao, X.Y., Huang, B., Wu, P.F., Li, Q., Li, H., Liu, Y.S., Cao, L.Y., *et al.* (2013). Elevated PLGF contributes to small-cell lung cancer brain metastasis. *Oncogene* 32, 2952–2962.

Lin, N.U., and Winer, E.P. (2007). Brain metastases: the HER2 paradigm. *Clin Cancer Res* 13, 1648-1655.

Lin, Q.B., K.; Fan, D.; Kim, S-J.; Guo, L.; Wang, H.; Bar-Eli, M.; Aldape, K. D.; Fidler, I. J. (2010). Reactive astrocytes protect melanoma cells from chemotherapy by sequestering intracellular calcium through gap junction communication channels. *Neoplasia* 12, 748-754.

Lorger, M., and Felding-Habermann, B. (2010). Capturing changes in the brain microenvironment during initial steps of breast cancer brain metastasis. *Am J Pathol* 176, 2958-2971.

Lutterbach, J., Bartelt, S., and Ostertag, C. (2002). Long-term survival in patients with brain metastases. *J Cancer Res Clin Oncol* 128, 417-425.

Maher, E.A., Mietz, J., Arteaga, C.L., DePinho, R.A., and Mohla, S. (2009). Brain metastasis: opportunities in basic and translational research. *Cancer Res* 69, 6015-6020.

Maness, P.F., and Schachner, M. (2007). Neural recognition molecules of the immunoglobulin superfamily: signaling transducers of axon guidance and neuronal migration. *Nat Neurosci* 10, 19-26.

McMahon, B., and Kwaan, H.C. (2008). The plasminogen activator system and cancer. *Pathophysiol Haemost Thromb* 36, 184-194.

Mechtersheimer, S., Gutwein, P., Agmon-Levin, N., Stoeck, A., Oleszewski, M., Riedle, S., Postina, R., Fahrenholz, F., Fogel, M., Lemmon, V., *et al.* (2001). Ectodomain shedding of L1 adhesion molecule promotes cell migration by autocrine binding to integrins. *J Cell Biol* 155, 661-673.

Meuwissen, R., Linn, S.C., Linnoila, R.I., Zevenhoven, J., Mooi, W.J., and Berns, A. (2003). Induction of small cell lung cancer by somatic inactivation of both Trp53 and Rb1 in a conditional mouse model. *Cancer Cell* 4, 181-189.

Minn, A.J., Gupta, G.P., Siegel, P.M., Bos, P.D., Shu, W., Giri, D.D., Viale, A., Olshen, A.B., Gerald, W.L., and Massagué, J. (2005). Genes that mediate breast cancer metastasis to lung. *Nature* 436, 518-524.

Moody, S.E., Sarkisian, C.J., Hahn, K.T., Gunther, E.J., Pickup, S., Dugan, K.D., Innocent, N., Cardiff, R.D., Schnall, M.D., and Chodosh, L.A. (2002). Conditional activation of Neu in the mammary epithelium of transgenic mice results in reversible pulmonary metastasis. *Cancer Cell* 2, 451-461.

Morita, S., Sato, A., Hayakawa, H., Ihara, H., Urano, T., Takada, Y., and Takada, A. (1998). Cancer cells overexpress mRNA of urokinase-type plasminogen activator, its receptor and inhibitors in human non-small-cell lung cancer tissue: analysis by Northern blotting and in situ hybridization. *Int J Cancer* 78, 286-292.

Muller, W.J., Sinn, E., Pattengale, P.K., Wallace, R., and Leder, P. (1988). Single-step induction of mammary adenocarcinoma in transgenic mice bearing the activated c-neu oncogene. *Cell* 54, 105-115.

Nayeem, N., Silletti, S., Yang, X., Lemmon, V.P., Reisfeld, R.A., Stallcup, W.B., and Montgomery, A.M. (1999). A potential role for the plasmin(ogen) system in the posttranslational cleavage of the neural cell adhesion molecule L1. *J Cell Sci* 112 (Pt 24), 4739-4749.

- Nguyen, D.X., Bos, P.D., and Massagué, J. (2009a). Metastasis: from dissemination to organ-specific colonization. *Nat Rev Cancer* 9, 274-284.
- Nguyen, D.X., Chiang, A.C., Zhang, X.H., Kim, J.Y., Kris, M.G., Ladanyi, M., Gerald, W.L., and Massagué, J. (2009b). WNT/TCF signaling through LEF1 and HOXB9 mediates lung adenocarcinoma metastasis. *Cell* 138, 51-62.
- Palmieri, D., Bronder, J.L., Herring, J.M., Yoneda, T., Weil, R.J., Stark, A.M., Kurek, R., Vega-Valle, E., Feigenbaum, L., Halverson, D., *et al.* (2007). Her-2 overexpression increases the metastatic outgrowth of breast cancer cells in the brain. *Cancer Res* 67, 4190-4198.
- Pang, P.T., Teng, H.K., Zaitsev, E., Woo, N.T., Sakata, K., Zhen, S., Teng, K.K., Yung, W.H., Hempstead, B.L., and Lu, B. (2004). Cleavage of proBDNF by tPA/plasmin is essential for long-term hippocampal plasticity. *Science* 306, 487-491.
- Perera, M., Ribot, E.J., Percy, D.B., McFadden, C., Simeone, C., Palmieri, D., Chambers, A.F., and Foster, P.J. (2012). In vivo magnetic resonance imaging for investigating the development and distribution of experimental brain metastases due to breast cancer. *Transl Oncol* 5, 217-225.
- Polleux, F., and Ghosh, A. (2002). The slice overlay assay: a versatile tool to study the influence of extracellular signals on neuronal development. *Sci STKE* 136, 19-29.
- Qian, Y., Hua, E., Bisht, K., Woditschka, S., Skordos, K.W., Liewehr, D.J., Steinberg, S.M., Brogi, E., Akram, M.M., Killian, J.K., *et al.* (2011). Inhibition of Polo-like kinase 1 prevents the growth of metastatic breast cancer cells in the brain. *Clin Exp Metastasis* 28, 899-908.
- Regales, L., Gong, Y., Shen, R., de Stanchina, E., Vivanco, I., Goel, A., Koutcher, J.A., Spassova, M., Ouerfelli, O., Mellinghoff, I.K., *et al.* (2009). Dual targeting of EGFR can overcome a major drug resistance mutation in mouse models of EGFR mutant lung cancer. *J Clin Invest* 119, 3000-3010.
- Schafer, M.K., and Altevogt, P. (2010). L1CAM malfunction in the nervous system and human carcinomas. *Cell Mol Life Sci* 67, 2425-2437.
- Schildge, S., Bohrer, C., Beck, K., and Schachtrup, C. (2013). Isolation and culture of mouse cortical astrocytes. *Journal of visualized experiments : JoVE*.
- Schmidt-Kittler, O., Ragg, T., Daskalakis, A., Granzow, M., Ahr, A., Blankenstein, T.J., Kaufmann, M., Diebold, J., Arnholdt, H., Muller, P., *et al.* (2003). From latent disseminated cells to overt metastasis: genetic analysis of systemic breast cancer progression. *Proc Natl Acad Sci U S A* 100, 7737-7742.
- Schouten, L.J., Rutten, J., Huveneers, H.A., and Tuijnstra, A. (2002). Incidence of brain metastases in a cohort of patients with carcinoma of the breast, colon, kidney, and lung and melanoma. *Cancer* 94, 2698-2705.
- Schreiber, R.D., Old, L.J., and Smyth, M.J. (2011). Cancer immunoediting: integrating immunity's roles in cancer suppression and promotion. *Science* 331, 1565-1570.
- Schroder, C., Schumacher, U., Fogel, M., Feuerhake, F., Muller, V., Wirtz, R.M., Altevogt, P., Krenkel, S., Janicke, F., and Milde-Langosch, K. (2009). Expression and prognostic value of L1-CAM in breast cancer. *Oncol Rep* 22, 1109-1117.
- Seike, T., Fujita, K., Yamakawa, Y., Kido, M.A., Takiguchi, S., Teramoto, N., Iguchi, H., and Noda, M. (2011). Interaction between lung cancer cells and astrocytes via specific inflammatory cytokines in the microenvironment of brain metastasis. *Clin Exp Metastasis* 28, 13-25.
- Siegel, P.M., Shu, W., Cardiff, R.D., Muller, W.J., and Massagué, J. (2003). Transforming growth factor beta signaling impairs Neu-induced mammary tumorigenesis while promoting pulmonary metastasis. *Proc Natl Acad Sci U S A* 100, 8430-8435.
- Silletti, S., Mei, F., Sheppard, D., and Montgomery, A.M. (2000). Plasmin-sensitive dibasic sequences in the third fibronectin-like domain of L1-cell adhesion molecule

- (CAM) facilitate homomultimerization and concomitant integrin recruitment. *J Cell Biol* **149**, 1485-1502.
- Sledge, G.W., Jr. (2011). HER2011: the changing face of HER2-positive breast cancer. *Clin Breast Cancer* **11**, 9.
- Sofroniew, M.V., and Vinters, H.V. (2010). Astrocytes: biology and pathology. *Acta Neuropathol Suppl (Berl)* **119**, 7-35.
- Steeg, P.S., Camphausen, K.A., and Smith, Q.R. (2011). Brain metastases as preventive and therapeutic targets. *Nat Rev Cancer* **11**, 352-363.
- Stemmler, H.J., Kahlert, S., Siekiera, W., Untch, M., Heinrich, B., and Heinemann, V. (2006). Characteristics of patients with brain metastases receiving trastuzumab for HER2 overexpressing metastatic breast cancer. *Breast* **15**, 219-225.
- Takehara, S., Onda, M., Zhang, J., Nishiyama, M., Yang, X., Mikami, B., and Lomas, D.A. (2009). The 2.1-Å crystal structure of native neuroserpin reveals unique structural elements that contribute to conformational instability. *J Mol Biol* **388**, 11-20.
- Teesalu, T., Hinkkanen, A.E., and Vaheri, A. (2001). Coordinated induction of extracellular proteolysis systems during experimental autoimmune encephalomyelitis in mice. *Am J Pathol* **159**, 2227-2237.
- Thies, A., Schachner, M., Moll, I., Berger, J., Schulze, H.J., Brunner, G., and Schumacher, U. (2002). Overexpression of the cell adhesion molecule L1 is associated with metastasis in cutaneous malignant melanoma. *Eur J Cancer* **38**, 1708-1716.
- Timmer, T., de Vries, E.G., and de Jong, S. (2002). Fas receptor-mediated apoptosis: a clinical application? *J Pathol* **196**, 125-134.
- Tischler, V., Pfeifer, M., Hausladen, S., Schirmer, U., Bonde, A.K., Kristiansen, G., Sos, M.L., Weder, W., Moch, H., Altevogt, P., *et al.* (2011). L1CAM protein expression is associated with poor prognosis in non-small cell lung cancer. *Mol Cancer* **10**, 127-137.
- Tsutsumi, S., Morohashi, S., Kudo, Y., Akasaka, H., Ogasawara, H., Ono, M., Takasugi, K., Ishido, K., Hakamada, K., and Kijima, H. (2011). L1 Cell adhesion molecule (L1CAM) expression at the cancer invasive front is a novel prognostic marker of pancreatic ductal adenocarcinoma. *J Surg Oncol* **103**, 669-673.
- Valastyan, S., and Weinberg, R.A. (2011). Tumor metastasis: molecular insights and evolving paradigms. *Cell* **147**, 275-292.
- Vanharanta, S., and Massagué, J. (2013). Origins of metastatic traits. *Cancer Cell* *in press*.
- Vos, Y.J., and Hofstra, R.M. (2010). An updated and upgraded L1CAM mutation database. *Hum Mutat* **31**, E1102-1109.
- Voura, E.B., Ramjeesingh, R.A., Montgomery, A.M., and Siu, C.H. (2001). Involvement of integrin alpha(v)beta(3) and cell adhesion molecule L1 in transendothelial migration of melanoma cells. *Mol Biol Cell* **12**, 2699-2710.
- Wang, X., Haroon, F., Karray, S., Martina, D., and Schluter, D. (2013). Astrocytic Fas ligand expression is required to induce T-cell apoptosis and recovery from experimental autoimmune encephalomyelitis. *Eur J Immunol* **43**, 115-124.
- Wiencken-Barger, A.E., Mavity-Hudson, J., Bartsch, U., Schachner, M., and Casagrande, V.A. (2004). The role of L1 in axon pathfinding and fasciculation. *Cereb Cortex* **14**, 121-131.
- Winslow, M.M., Dayton, T.L., Verhaak, R.G., Kim-Kiselak, C., Snyder, E.L., Feldser, D.M., Hubbard, D.D., DuPage, M.J., Whittaker, C.A., Hoersch, S., *et al.* (2011). Suppression of lung adenocarcinoma progression by Nkx2-1. *Nature* **473**, 101-104.
- Yepes, M., Sandkvist, M., Wong, M.K., Coleman, T.A., Smith, E., Cohan, S.L., and Lawrence, D.A. (2000). Neuroserpin reduces cerebral infarct volume and protects neurons from ischemia-induced apoptosis. *Blood* **96**, 569-576.

Zhu, C.Q., Ding, K., Strumpf, D., Weir, B.A., Meyerson, M., Pennell, N., Thomas, R.K., Naoki, K., Ladd-Acosta, C., Liu, N., *et al.* (2010). Prognostic and predictive gene signature for adjuvant chemotherapy in resected non-small-cell lung cancer. *J Clin Oncol* 28, 4417-4424.

FIGURE LEGENDS

Figure 1. Association of PA-inhibitory serpins with the brain metastatic phenotype

(A) Serpin mRNA levels in brain metastatic cell lines relative to the levels in counterparts not metastatic to brain. qRT-PCR values are averages of at least three independent reactions. Sources of the metastatic cells are indicated. TN, triple negative breast cancer; ER-, estrogen receptor negative, PR-, progesterone receptor negative. (B) qRT-PCR analysis of the indicated serpins in the parental MDA231 cell line and derivatives with metastatic tropism to bone, lung, or brain. Error bars, 95% confidence interval. (C) Representative ex vivo bioluminescence (BLI) images of brains from immunocompetent mice inoculated with different *Kras*^{G12D};*p53*^{-/-} mouse lung cancer cell lines. The percentage of mice developing brain metastasis and the mean BLI photon flux signal are indicated. n=10 (D) Heatmap of serpin mRNA expression in *Kras*^{G12D};*p53*^{-/-} derivatives based on qRT-PCR analysis. (E) Summary of the serpin-PA-plasmin cascade. (F) Inhibition of plasminogen conversion into plasmin by cell culture supernatants of the indicated cell lines. Plasmin activity was determined by a chromogenic assay. Data are averages ± SEM from triplicate experiments. (G) Kaplan-Meier analysis of brain metastasis-free survival in 106 cases of lung adenocarcinoma classified based on *SERPINB2* and *SERPINI1* mRNA levels in the primary tumor. P value calculated from a Cox proportional hazard model, with *SERPINB2* and *SERPINI1* expression treated as a continuous variable. (H) Representative human brain metastasis samples from lung and breast cancer stained with antibodies against neuroserpin or serpin B2. (I) Proportion of metastasis samples scoring positive for neuroserpin immunostaining (red) or serpin B2 immunostaining (orange) in 33 cases of non-small cell lung carcinoma and 123 cases of breast carcinoma. Small diagrams in the breast cancer set represent the primary tumor subtype (TN, triple negative; HER2, HER2+; ER/PR, hormone-receptor positive; TP, triple positive) of the serpin-positive samples for which this information was available. Brain metastases scoring positive for both serpins comprise 42% and 34% of the lung cancer and breast cancer cases, respectively. Samples scored as positive had >80% of neoplastic cells showing positive reactivity. Scale bar: 100µm.

Figure 2. Vascular cooption, outgrowth, and escape from stromal plasmin action

(A) Metastatic cell interactions with brain capillaries. MDA231-BrM2 cells (green) remain bound to brain capillaries (red) after completing extravasation. (B) Confocal analysis of

the extravasation steps showing an MDA231-BrM2 cell lodged intravascularly in a brain capillary, a cell transiting through the capillary wall, and an extravasated cell that is spreading over the abluminal capillary surface. (C) Cluster of extravasated MDA231-BrM2 cells forming a furrow around a brain capillary. All extravasated cells initially grew in this manner. Red or magenta, collagen IV in vasculature. Green, GFP. Blue, nuclear staining with bis-benzamide. (D) Schema representing the initial steps and interactions during metastatic colonization of the brain. (E) Exposure of metastatic H2030-BrM3 cells to GFAP⁺ reactive astrocytes (arrowheads) in the brain parenchyma at different time points after inoculation of cancer cells into the circulation. Day 3: red, collagen IV; white, GFAP; green, GFP⁺ cancer cells. Day 7 onwards: red, GFAP; green, GFP; blue, nuclear staining. (F,G) tPA and uPA immunofluorescence staining (red, arrowheads) associated with GFAP⁺ astrocytes (blue) in a mouse brain harboring GFP⁺ H2030-BrM3 cells (green). (H) Plasminogen immunofluorescence staining (white, arrowheads) is associated with NeuN⁺ neuron bodies (red) near a cluster of GFP⁺ metastatic cells (green) in a mouse brain. Blue, nuclear staining. (I) Schema of brain slice organotypic cultures. Cancer cells placed on the surface of slices migrate into the tissue and seek microcapillaries. (J) Representative image of a brain slice harboring infiltrated H2030-BrM3 cells that are still round (open arrowheads) or already spread over brain capillaries (closed arrowheads). (K) Representative confocal images of brain slice tissue infiltrated with the indicated cancer cells. α 2-antiplasmin was added to the indicated cultures. Note the lower density and disorganized aspect of parental cells compared with the stretched morphology of BrM3 cells or parental cells with α 2-antiplasmin. (L) Quantification of GFP⁺ cancer cells in the experiments of panel K. Number of cells per field of view (FOV) are averages \pm SEM. n=6-10 brain slices, scoring at least two fields per slice, in at least 2 independent experiments. (M) Cleaved caspase-3 immunofluorescence staining in brain slices harboring the indicated cells and additions. (N) Quantification of cleaved caspase-3 positive cancer cells in the experiments of panel M. Values are normalized to H2030-BrM3, and are averages \pm SEM. n=6-10 brain slices, scoring at least two fields per slice, from at least 2 independent experiments. (O) Schematic summary showing neurons and astrocytes as sources of plasminogen and PA, respectively, and lethal effect of the resulting plasmin on infiltrating cancer cells. All P values by Student's t-test. Scale bars: 25 μ m (A), 5 μ m (B-C), 5 μ m (Day 3), 15 μ m (Day 7), 25 μ m (Day 14), 70 μ m (micrometastasis), 100 μ m (macrometastasis) (D), 10 μ m (F-H), 100 μ m (K), 5 μ m (M)

Figure 3. Neuroserpin mediates brain metastasis

(A) Schema of experimental design. Brain metastases develop in mice after inoculation of cancer cells into the arterial circulation. Brain lesions are analyzed by bioluminescence imaging (BLI) based on the expression of firefly luciferase in cancer cells and by immunofluorescence (IF) based on the expression of GFP. (B) Representative images of whole-body BLI and brain ex vivo BLI 5 weeks after inoculation of H2030-BrM3 cells transduced with control shRNA or *neuroserpin* shRNA (shNS). (C) Kaplan–Meier plot of brain metastasis-free survival in the experiment of panel B. Control (n=20) and two different shNS [shNS (1), n=11; shNS (2), n=13] were analyzed. P values were obtained with log rank Mantel-Cox test. (D) Quantification of ex vivo BLI in brains from panel B. (E) Representative images of coronal brain sections analyzed for GFP IF 21 or 35 days after inoculation of H2030-BrM3 cells into mice. Lesion contours are marked. (F) Quantification of brain lesions according to size at 21 day time point in panel E. Control n=5, shNS n=6 brains. P value refers to size distribution. For the total number of lesions, $p < 0.05$. (G) Quantification of brain tumor burden in the experiment of panel E. Control n=5, shNS n=6. (H) Representative images of control and *neuroserpin*-depleted H2030-BrM3 cells in brain slice assays. Insets show cleaved caspase-3 immunofluorescence. (I) Quantification of GFP+ cells in the experiment of panel H. Data are averages \pm SEM. n=6-10 slices, scoring at least two fields per slice, in at least 2 independent experiments. (J) Quantification of cells that were positive for cleaved caspase-3 in the experiment of panel H. Values were normalized to the control group. Data are averages \pm SEM. n=6-10 slices, scoring at least two fields per slice, from at least 2 independent experiments. (K,L) Quantification of cells that were positive for cleaved caspase-3 comparing parental and BrM cell lines, and the effect of overexpressing neuroserpin wild type or a mutant form unable to target PA ($NS^{\Delta loop}$) in parental cell lines H2030 (K) and MDA231 (L). Values were normalized to the corresponding BrM cell lines. Data are averages \pm SEM. n=6-10 slices, scoring at least two fields per slice, from at least 2 independent experiments. (M) Representative ex vivo BLI images of brains and hindlimbs from mice 21 days after inoculation with PC9-BrM3. Cells were transduced with empty vector (n=5) or vectors encoding wild type neuroserpin (n=7) or $\Delta loop$ neuroserpin mutant (n=8). (N) Ratio of photon flux in brain versus bone in the experiment of panel M. Ex vivo brain mean BLI values are also shown. All P values were calculated by Student's t-test, except in panel C. Scale bar:

250µm (E), 100µm, 5µm (inset) (H).

Figure 4. Anti-PA serpins mediate brain metastasis by breast cancer cells

(A,B) MDA231-BrM2 cells transduced with control vector, shRNA vectors targeting *neuroserpin*, *SERPINB2* and *SERPIND1* (triple K/D), *SERPINB2* shRNA (shSB2), or shSB2 plus a neuroserpin expressing vector were inoculated into the arterial circulation of immunodeficient mice. Brain metastasis burden was visualized by ex vivo brain BLI (A) and quantitated (B). Control n=22; triple K/D n=9, shSB2 n=14; shSB2 and neuroserpin n=8. (C) Distribution of clones (single cell progenies –SCP-) overexpressing one, two, or three of the indicated serpins among ten clonal cell lines isolated from the MDA231-BrM2 population. (D) Ex vivo brain BLI quantification from different MDA231-BrM2 SCP injected. Red dots SCP (high levels of all serpins), n=8; light green dots SCP (low levels of serpin B2), n=11; blue dots SCP (low levels of serpin B2 and D1), n=8; dark green dots SCP (low levels of serpin B2 and neuroserpin), n=5. P value was determined by Student's t-test. (E) SCP with high levels of neuroserpin and serpin D1, were subjected to *neuroserpin* knock down and tested for brain metastatic activity. Metastatic load was quantitated by ex vivo brain BLI after 21 days. (F) Kaplan–Meier survival curves for brain metastasis-free survival in immunocompetent mice inoculated with congenic parental ErbB2-P cells (n=9) or brain metastatic derivatives ErbB2-BrM1 (n=7) and ErbB2-BrM2 (n=5). Survival curves were compared using log rank Mantel-Cox test. ErbB2-P versus ErbB2-BrM1, $P=0.0045$, and versus ErbB2-BrM2 $P=0.0053$. (G) Representative whole body BLI images of metastatic lesions formed by ErbB2-BrM2 or these cells expressing a serpin B2 shRNA. (H) Quantification of brain BLI photon flux in the experiment of panel G. Control ErbB2-BrM2 cells (n=10), and the same cells expressing two different serpin B2 shRNAs, shSB2 (1), n=10; shSB2 (2), n=6, were analyzed. Data are averages \pm SEM. All P values were determined by Student's t-test, except in panel G.

Figure 5. Neuroserpin shields cancer cells from FasL death signals

(A) Schema of FasL and its conversion by plasmin into sFasL, a diffusible trigger of apoptosis through Fas-FADD signaling. TMD, transmembrane domain; SA, trimeric self-assembly domain; THD, tumor necrosis factor-homology domain. Red crosses, apoptotic cells. a, astrocyte. c, cancer cell. (B) Immunofluorescence with antibodies against GFP

(cancer cells, green), GFAP (reactive astrocytes, blue) and FasL (magenta) in a mouse brain harboring metastatic cells 21 days after arterial inoculation of H2030-BrM3. (C) Images of astrocyte cultures incubated with exogenous plasminogen (1 μ M) or no additions. Immunofluorescence staining was performed with antibodies against the extracellular domain (ECD) or the intracellular domain of FasL (ICD). (D) Western immunoblotting of supernatants from cultures shown in panel C, using anti-FasL ECD antibodies. Tubulin was used as loading control. (E) Mouse brain slices were incubated with α 2-antiplasmin, neuroserpin and serpin B2, or no additions. sFasL in tissue lysates was detected by western immunoblotting analysis with anti-FasL ECD antibodies. (F) GFP+ H2030-BrM3 cells (green) were allowed to infiltrate brain slices in media containing added sFasL or no additions. With sFasL the cancer cells scored positive for apoptosis marker cleaved caspase-3 (red, in inset). (G, H) Quantification of total GFP+ cell numbers (G), and apoptotic GFP+ cells (H) in the experiments of panels F (orange bars) and I (green bars). Data are averages \pm SEM. n=6-10 slices, scoring at least two fields per slice, from at least 2 independent experiments. (I) GFP+ H2030 cells (green) were allowed to infiltrate brain slices in media containing anti-FasL blocking antibody or no additions. Anti-FasL prevented endogenous signals from triggering caspase-3 activation (red, in inset). (J) Depiction of FADD-DD overexpression (yellow shape) to suppress pro-apoptotic Fas signaling in cancer cells. (K) qRT-PCR analysis of *FADD* expression in H2030-BrM3 transduced with a FADD-DD vector, a *neuroserpin* shRNA vector, or empty vector, as indicated. (L) Quantification of apoptotic cells following sFasL addition to H2030-BrM3 cells transduced with the indicated vectors. (M, N) Quantification of total GFP+ cells (M), and apoptotic GFP+ cells (N) in brain slices harboring the indicated GFP+ H2030-BrM3 transfectants and/or additions. Data are averages \pm SEM. n=5-8 slices, scoring at least two fields per slice, from at least 2 independent experiments. (O) Brain metastatic activity of H2030-BrM3 cells transduced with the indicated vectors and inoculated into the arterial circulation of mice. BLI photon flux was quantitated in cells transduced with control shRNA (n=11), FADD-DD (n=4), *neuroserpin* shRNA (n=14), or this shRNA and FADD-DD (n=12). All P values were determined by Student's t-test. Scale bars: 25 μ m (B), 200 μ m (C), 100 μ m (F,I), 5 μ m (insets in F,I).

Figure 6. The plasmin target L1CAM mediates vascular cooption by brain metastatic cells

(A) Schema of L1CAM as a mediator of homophilic and heterophilic (e.g., integrins) cell adhesive interactions, and its conversion by plasmin into an adhesion defective fragment. Immunoglobulin-like (Ig) and fibronectin type III (FNIII) domain repeats, the intracellular domain (ICD), and an integrin-binding RGD sequence are indicated. (B) Suspensions of GFP+ H2030-BrM3 cells were placed on top of a monolayer of human brain microvascular endothelial cells (HBMEC), and HBMEC-bound cancer cells were imaged 20 min later for GFP, L1CAM immunostaining, and nuclear staining with bis-benzamide. L1CAM is highly expressed in the cancer cells and at lower level in the HBMECs. (C, D) Analysis of H2030-BrM3 binding to HBMEC monolayers (C) or to H2030-BrM3 monolayers (D), and effect of L1CAM knockdown. Data are averages \pm SEM. n=5, scoring at least 10 fields per coverslip. (E) Flow cytometric analysis of cell-surface L1CAM in the indicated brain cells expressing *L1CAM* shRNA or incubated with plasmin, compared to untreated controls. (F) Anti-L1CAM western immunoblotting analysis of cells and culture supernatants after incubation with or without plasmin. (G,H) Cancer cells were treated with plasmin and subjected to HBMEC adhesion assays. Data are averages \pm SEM. n=3, scoring at least 5 fields per coverslip. (I) Control or *L1CAM*-depleted H2030-BrM3 cells after infiltrating brain tissue slices. GFP+ cancer cells (green) and vasculature (collagen IV immunostaining, red) were visualized after 2 days. Two representative images are shown per condition. Lower panels, high magnification. (J,K) Quantification of cells that were spread on capillaries (J) and Ki67+ cells (K) in the experiments of panel I. Data are averages \pm SEM. n=6 slices, scoring at least three fields per slice, from 2 independent experiments. (L) Effect of neuroserpin overexpression and *L1CAM* depletion on the interaction of PC9-BrM3 cells with capillaries in brain slices. (M,N) Quantification of cells that were spread on capillaries (M) and Ki67+ cells (N) in the experiments of panel L. Data are averages \pm SEM. n=6 slices, scoring at least three fields per slice, from 2 independent experiments. All P values by Student's t-test. Scale bars: 10 μ m (B), 50 μ m (I,L).

Figure 7. L1CAM mediates metastatic outgrowth in the brain.

(A) Immunohistochemical staining with anti-L1CAM antibodies and H&E counterstaining of incipient brain colonies formed by H2030-BrM3. Cancer cells (cc, pale blue nuclei) remain close to each other and interact with endothelial cells (e, dark blue nuclei). Insets, higher magnification of cell-cell contact areas. (B) Ex vivo BLI of representative brains from mice that were arterially inoculated with indicated H2030-BrM3 cells. (C)

Quantification of ex vivo brain photon flux in the experiments of panel B. Control shRNA, n=9; shL1CAM, n=6. (D) Quantification of ex vivo BLI of brains from mice that were arterially inoculated with indicated MDA231-BrM2 cells. Control shRNA, n=9; shL1CAM, n=10. (E) H2030-BrM3 cells infiltrating the brain 7 days after intracardiac injection, and effect of L1CAM depletion. (F) Representative images of GFP+ metastatic lesions from brains in panel C. (G) Relative abundance of macrometastasis over micrometastasis (as defined in Figure 3F) in brains shown in panel C. Number of lesions: control= 283.2 ± 84.8 , shL1CAM= 69.8 ± 11.5 . Data are averages \pm SEM. n=3 brains. (H) Quantification of ex vivo BLI photon flux of brains from mice that were arterially inoculated with the indicated PC9-BrM3 cells (n=5-7). All P values were determined by Student's t-test. Scale bar: 25 μ m (A), 30 μ m (E), 200 μ m (F). (I) Model of the action of the stromal PA-plasmin system against cancer cells that infiltrate the brain, and role of anti-PA serpins in protecting brain metastatic cells from stromal PA-plasmin. Reactive astrocytes produce PAs in the presence of extravasated cancer cells. Metastasis fails (left side) when PAs generate plasmin from neuron-derived plasminogen and plasmin mobilizes FasL from astrocytes to kill cancer cells. Additionally, plasmin cleaves and inactivates L1CAM, a cell adhesion molecule that cancer cells express for vascular cooption. Metastasis proceeds (right side) when brain metastatic cells express anti-PA serpins that prevent the generation of plasmin and its deleterious effects on the survival and vascular attachment of the cancer cells.

Supplementary Figures

Figure S1. Highly expressed genes in brain metastasis models and clinical samples. Related to Figure 1.

(A) Genes that were previously associated with brain metastatic activity in two lung adenocarcinoma brain metastasis models (H2030-BrM3 and PC9-BrM3; Nguyen et al, 2009) or two breast cancer brain metastasis models (MDA231-BrM2 and CN34-BrM2; Bos et al, 2009) and found to be shared among these models. Values indicate fold-increase in the expression of these genes in BrM cells compared to non-brain metastatic counterparts in GeneChip transcriptional data sets (Nguyen et al. 2009, Bos et al, 2009).

(B) Cell lines derived from genetically engineered *Kras*^{G12D};*p53*^{-/-} mouse lung tumors (373N1, 393N1, 482N1, 2691N1) were tested for overall metastatic activity from the arterial circulation in syngeneic mice. Kaplan-Meier plots of metastasis-free survival, n=10 mice per cell line. All cell lines showed multiorgan metastatic activity as previously described (Winslow et al, 2011), but differed in brain metastatic activity (see Figure 1).

(C) Neuroserpin (NS) protein levels in low-serum cell culture supernatants, as determined by ELISA. (D) Serpin B2 (SB2) protein levels in cell lysates determined by western immunoblotting. (E) Plasminogen conversion into plasmin was inhibited to different extents by cell culture supernatants from the indicated cells lines. Plasmin activity was determined by a chromogenic assay. P values were determined by Student's t-test. * $P < 0.05$, *** $P < 0.001$.

(F,G) Kaplan-Meier analysis of bone metastasis-free survival and contralateral lung metastasis-free survival in 106 cases of lung adenocarcinoma classified based on *SERPINB2* and *SERPINI1* mRNA levels in the primary tumor. P value calculated by a Cox proportional hazard model, with *SERPINB2* and *SERPINI1* expression treated as a continuous variable. (H) Kaplan-Meier analysis of brain metastasis-free survival in 615 cases of breast adenocarcinoma (EMC-MSK dataset) classified based on *SERPINB2* and *SERPINI1* mRNA levels in the primary tumor. P value calculated from a Cox proportional hazard model, with *SERPINB2* and *SERPINI1* expression treated as a continuous variable. (I) Immunohistochemistry against NS and SB2 in brains from mice intracardially inoculated with indicated cell lines. (J) Representative brain metastasis tissue microarray cores stained with neuroserpin or serpin B2 antibodies. Scale bar: 100 μ m.

Figure S2. Interactions of metastatic cells with the brain parenchyma. Related to

Figure 2.

(A) Experimental design for the analysis of brain metastatic colonies formed by circulating cancer cells. (B) Quantification of parental MDA231 (P) and MDA231-BrM2 (BrM) cells in the brain at the indicated times after inoculation into the arterial circulation of mice. Data are averages \pm SEM of multiple fields in 2 brains. P values were determined by Student's t-test comparing cells extravasated in the parental and brain metastatic populations before and after 7 days. (C,D) Cells (vimentin+, green) that remained in the lumen of brain capillaries (collagen IV positive) 7 days after inoculation scored positive for cleaved caspase-3 immunofluorescence (red, arrowhead in D). (E,F) Non reactive astrocytes (E), located in uninvolved areas and reactive astrocytes in areas that contain metastatic cells (F) can be distinguished based on dramatic morphological changes, including modified interaction with capillaries, and the thickening and reduction in the number of cellular processes. (G-J) Interaction of H2030-BrM3 cells with different components of the brain microenvironment including reactive microglia (Iba1+) and neurons (NeuN+) from extravasation through overt metastasis. (K) D-VLK chromogenic plasmin substrate assay was used to compare the plasmin activity associated with mouse microglia or astrocyte culture supernatants. (L) Quantification of cleaved caspase-3 positive cancer cells in co-cultures with glial cells with added plasminogen. Values are normalized to H2030-BrM3 without plasminogen, and are averages \pm SEM. n=6-9 co-cultures per condition, scoring multiple fields per co-culture, from 3 independent experiments. (M) Quantification of cleaved caspase-3 positive cancer cells in brain slice assays. Values are normalized to MDA231-BrM2, and are averages \pm SEM. n=6-10 brain slices, from 2 independent experiments. (N) Schema of experimental design to analyze plasmin activity in brain slices. (O) α 2-antiplasmin inhibition of plasmin in brain slices. (P) Plasmin addition to H2030 cells in monolayer culture does not induce cell death. All P values were determined by Student's t-test. Scale bars: 10 μ m (C), 50 μ m (E,F), 20 μ m (G,I), 500 μ m (H,J).

Figure S3. Neuroserpin mediates brain metastasis by lung cancer cells. Related to Figure 3.

(A) Neuroserpin IF (red) in brains harboring GFP+ H2030-BrM3 metastasis (green). Insets show colocalization (yellow) of neuroserpin with GFP+ cancer cells. (B) *Neuroserpin* mRNA levels as determined by qRT-PCR in H2030-BrM3 and derivatives

transduced with *neuroserpin* shRNAs. (C) Neuroserpin ELISA was performed on culture supernatants of the indicated H2030 derivatives. (D) MTT cell proliferation assays of H2030-BrM3 cells transduced with control or *NS* shRNA. (E) Tracings and size distribution of metastatic lesions in the brain of animals from Figure 3D. Relative abundance of each size group is shown for every experimental condition. (F) The few macrometastases that were formed by *neuroserpin*-depleted H2030-BrM3 cells scored positive for neuroserpin IF (left panels), whereas micrometastases scored negative for neuroserpin (right panels). (G) *Neuroserpin* knockdown in H2030-BrM3 did not alter the number of extravasated cells on day 7 after inoculation. Data are averages \pm SEM from 3 brains. (H) Schema of the assay for cancer cell transmigration through an experimental blood-brain barrier (BBB) (Bos et al., 2009). HUVEC, primary human umbilical vein endothelial cells. (I) Quantification of cells that migrated through this experimental BBB normalized to H2030-BrM3 control cells. An shRNA targeting the brain extravasation mediator *ST6GalNaC5* (Bos et al., 2009) served as positive control (shNS vs sh*ST6GalNaC5*, $P < 0.001$). At least 5 independent migration assays were performed for each condition. (J) qRT-PCR analysis of *neuroserpin* mRNA levels in PC9-BrM3 cells that were transfected with the indicated flag epitope-tagged neuroserpin constructs. PCR primer set #1 recognizes only the wild type *neuroserpin* mRNA, whereas set #2 recognizes both the wild type and the Δ loop mutant forms. (K) Neuroserpin ELISA was performed on culture supernatants of PC9-BrM3 or this cell line expressing a neuroserpin cDNA. (L) Anti-flag western immunoblotting of culture supernatants from PC9-BrM3 cells expressing the indicated neuroserpin constructs. Tubulin immunoblotting was used as loading control. (M) Proliferation assays of control and neuroserpin overexpressing PC9-BrM3 cells. All P values by Student's t-test. Scale bars: 200 μ m (A,F), 100 μ m (A, inset), 250 μ m (E).

Figure S4. Analysis of multiple coexpressed serpins in MDA231-BrM2 cells.

Related to Figure 4.

(A) qRT-PCR of MDA231-BrM2 expressing shRNAs that target the three indicated serpins. (B) Neuroserpin ELISA in low serum culture supernatant from the indicated cell lines. (C) Anti-serpin B2 (SB2) western immunoblotting of lysates from the indicated cell lines. (D) Proliferation assays of shSB2 MDA231-BrM2 transduced cell lines. (E) Anti-serpin B2 western immunoblotting of lysates from the indicated cells lines. BrM2-SCP^{HIGH} and BrM2-SCP^{LOW} correspond to clonal lines from MDA231-BrM2 as shown in

Figure 4D. (F) Neuroserpin ELISA of culture supernatant from the indicated cell lines. (G) Kaplan–Meier plot of brain metastasis-free survival comparing MDA231-BrM2 control (n=5) and shNS (1) (n=9). P values by log rank Mantel-Cox test. (H) Kaplan–Meier plot of brain metastasis-free survival comparing CN34-BrM2 control (n=12) and shSERPINE2 (1) (n=5) were analyzed. P values by log rank Mantel-Cox test. (I) qRT-PCR analysis of serpin expression in single-cell progenies (SCP) isolated from the MDA231-BrM2 cell line. Black, clonal lines; blue, parental population; orange, BrM population. (J) Ex vivo BLI images of representative brains from metastasis assays of MDA231-BrM2 SCP expressing the indicated serpins quantified in Figure 4D.

Figure S5. sFasL triggers apoptosis in brain metastatic cells. Related to Figure 5.

(A) High magnification of an astrocyte stained with anti-GFAP and anti-FasL antibodies in a brain lesion formed by H2030-BrM3 cells. (B) qRT-PCR analysis of *FasL* mRNA levels in primary cultures of mouse astrocytes and microglia. Data are averages of triplicates \pm SEM. (C) Schema showing the various anti-FasL antibodies used. (D,E) Quantification of FasL ECD and ICD immunofluorescence signals in Figure 5C. (F) Anti-Fas western immunoblotting of indicated cell lysates. Tubulin immunoblotting was used as loading control. (G) Cleaved caspase-3 IF (red) in breast (CN34-BrM2) and lung (H2030-BrM3) brain metastatic cell monolayers that were incubated with or without addition of sFasL (500ng/ml). Blue, nuclear staining. (H) Quantification of the experiment shown in panel G, at the indicated concentrations of sFasL. Data are averages \pm SEM of three independent experiments. All differences with control were $P < 0.01$, as determined by Student's t-test. (I) Cell proliferation assays of the indicated cell lines with or without addition of sFasL (500ng/ml). Data are averages of triplicates \pm SEM. P values were determined for the difference on day 6, by Student's t-test. (J) Quantification of cleaved caspase-3 positive H2030 cancer cells in brain slices treated with added $\alpha 2$ -antiplasmin, $\alpha 2$ -antiplasmin and sFasL, or no additions. Values are normalized to H2030+ $\alpha 2$ -antiplasmin, and are averages \pm SEM. n=5-8 brain slices, scoring at least two fields per slice, from at least 2 independent experiments. (K) qRT-PCR analysis of *neuroserpin* mRNA levels in H2030-BrM3 cells that were transduced with FADD-DD and *neuroserpin* shRNA vectors as indicated. (L) Quantification of cleaved caspase-3 positive MDA231-BrM2 cancer cells in brain slices. MDA231-BrM2 cells were transduced with a control vector, serpin B2 (*SB2*) shRNA, or this shRNA plus a FADD-DD expression vector. Values are normalized to MDA231-BrM2 control, and are averages \pm SEM. n=6-10 brain

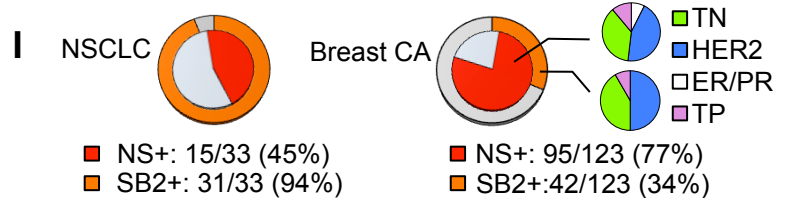
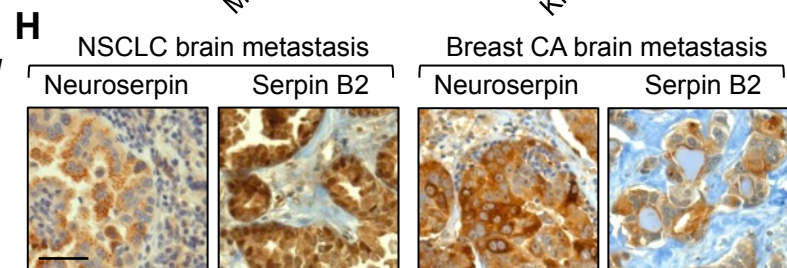
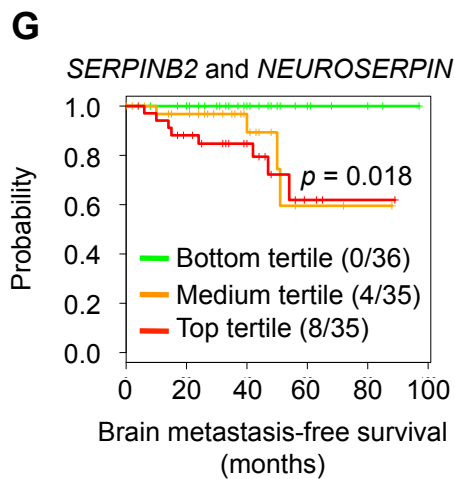
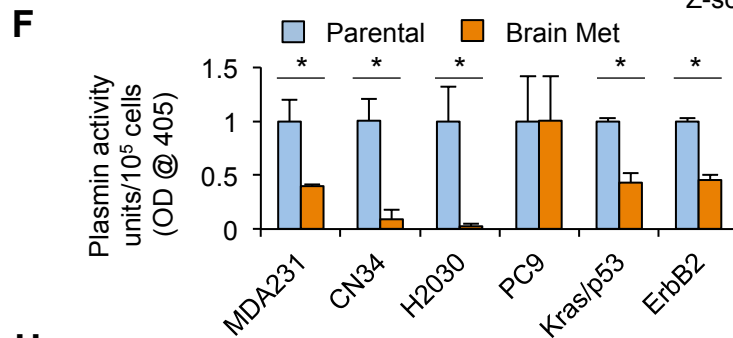
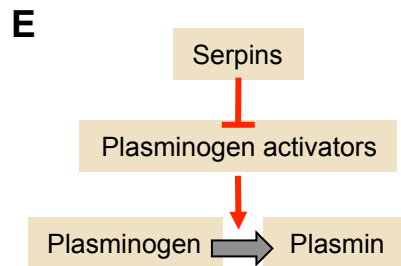
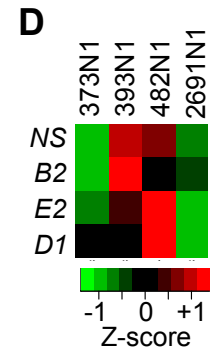
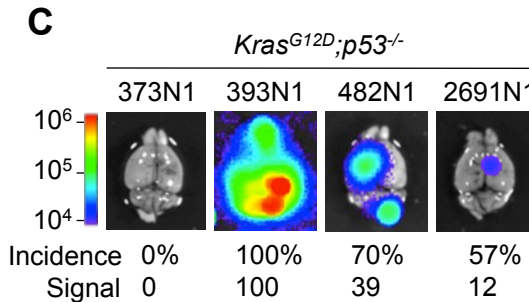
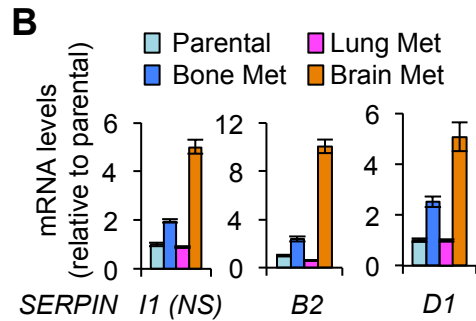
slices, scoring at least two fields per slice, from at least 2 independent experiments. All P values by Student's t-test. Scale bars: 1 μ m (A), 100 μ m (G).

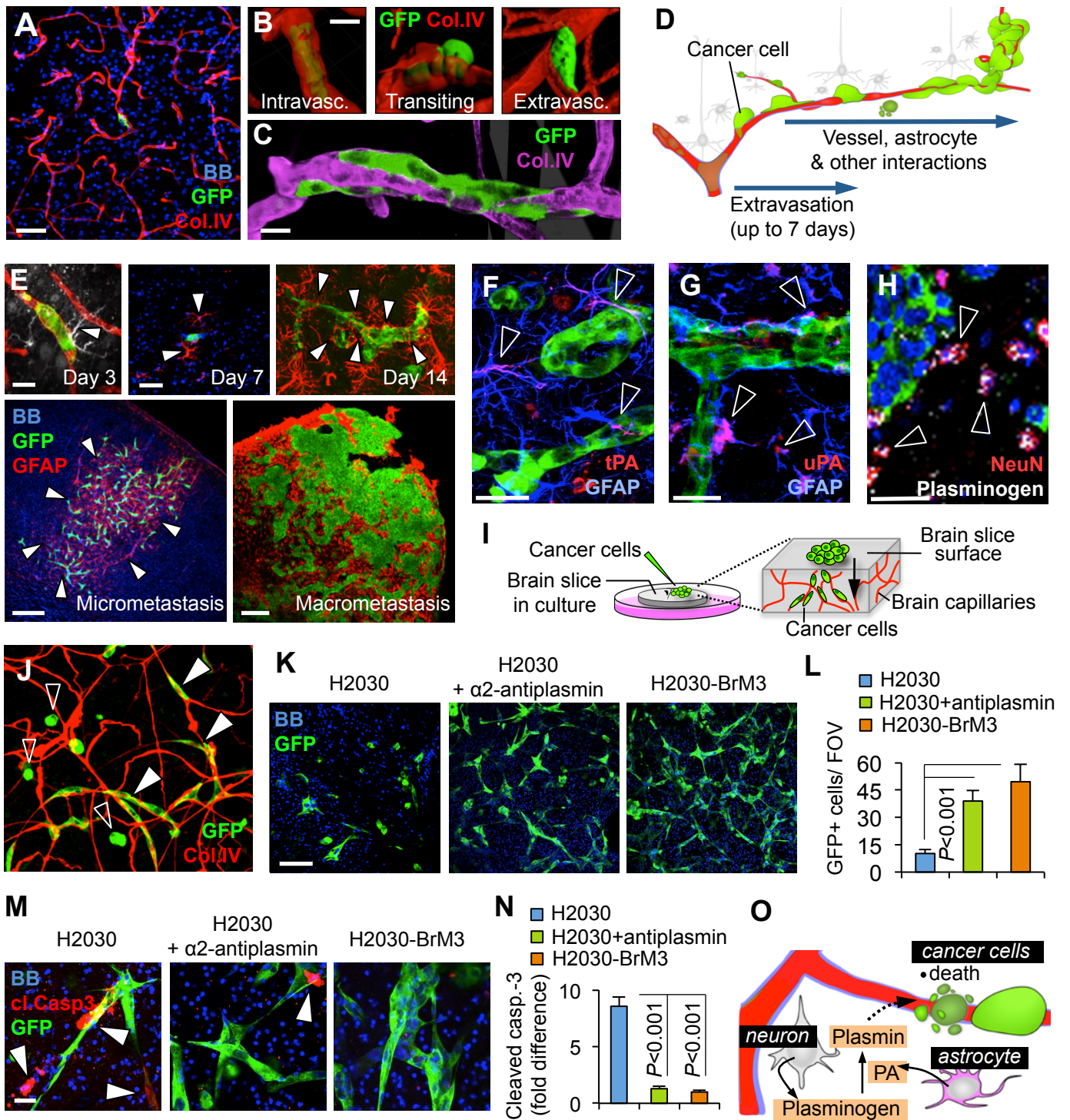
Figure S6. L1CAM as a plasmin target and a mediator of brain metastasis. Related to Figure 6.

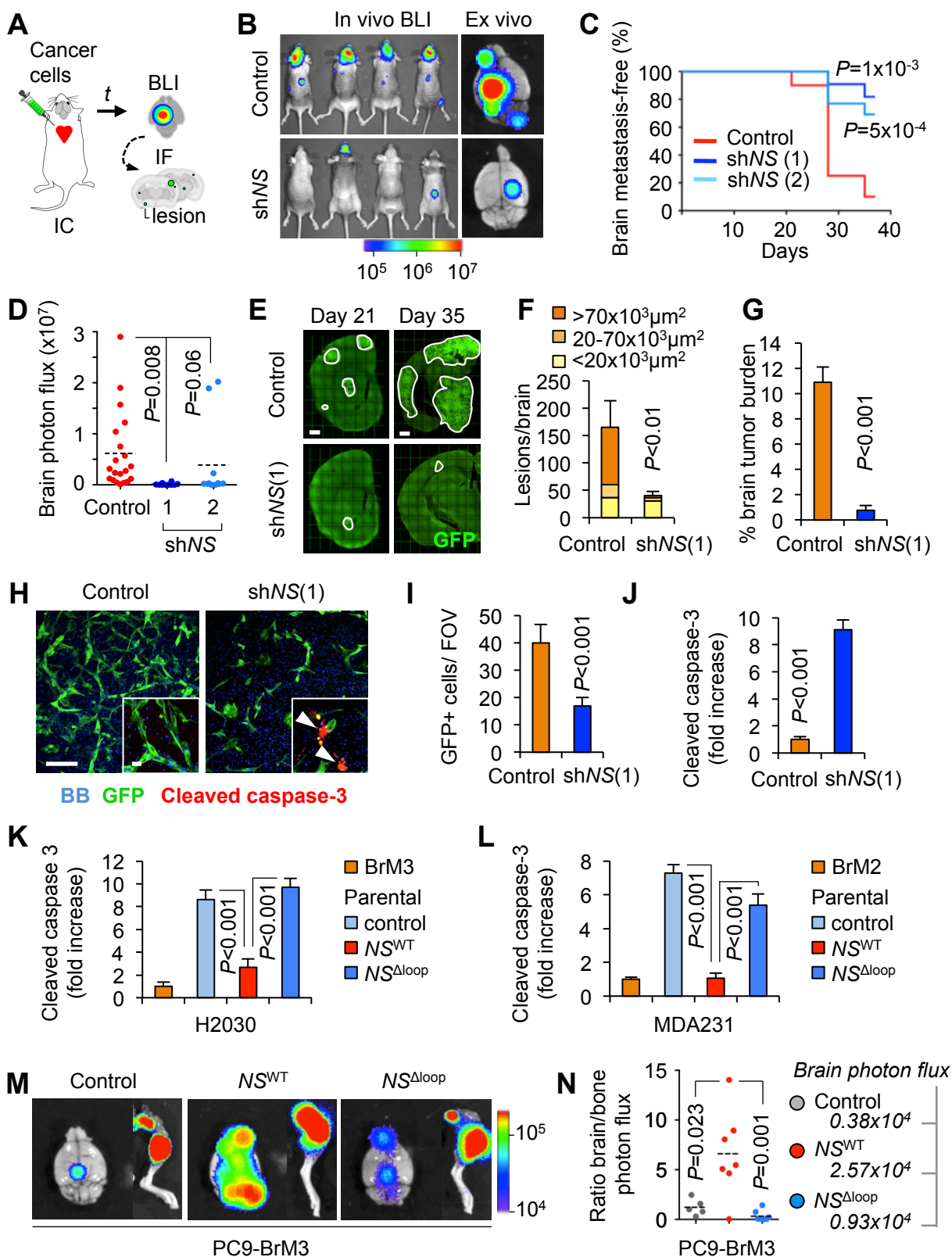
(A) Representative GFP IF images from brains harboring lesions formed by the indicated cell lines. Scale bar: 100 μ m, 25 μ m (insets). (B,C) Anti-L1CAM western immunoblotting of cell lysates for the indicated human (B) and murine (C) lung or breast cancer cell lines. (D) MTT proliferation assay of control and *L1CAM*-depleted H2030-BrM3 cells. (E) Quantification of GFP+ cancer cells that were in contact with, but not necessarily spread on brain capillaries in the experiments of Figure 6I. Ten fields (>180 individual cells) were scored per condition. Data are averages \pm SEM. (F) Quantification of apoptotic wild type or *L1CAM*-depleted H2030-BrM3 cells in brain slice assays. Data are averages \pm SEM. n=5-8 slices from two independent experiments, and at least two fields were scored per slice. (G) Quantification of MDA231-BrM2 control or sh*L1CAM* transduced cells that were spread on capillaries. Data are averages \pm SEM. n=6 slices, scoring at least three fields per slice, from 2 independent experiments. (H,I) qRT-PCR analysis of *L1CAM* (H) and *neuroserpin* (I) mRNA levels in PC9-BrM3 cells that were transduced with neuroserpin expression vector and/or *L1CAM* shRNA vector as indicated.

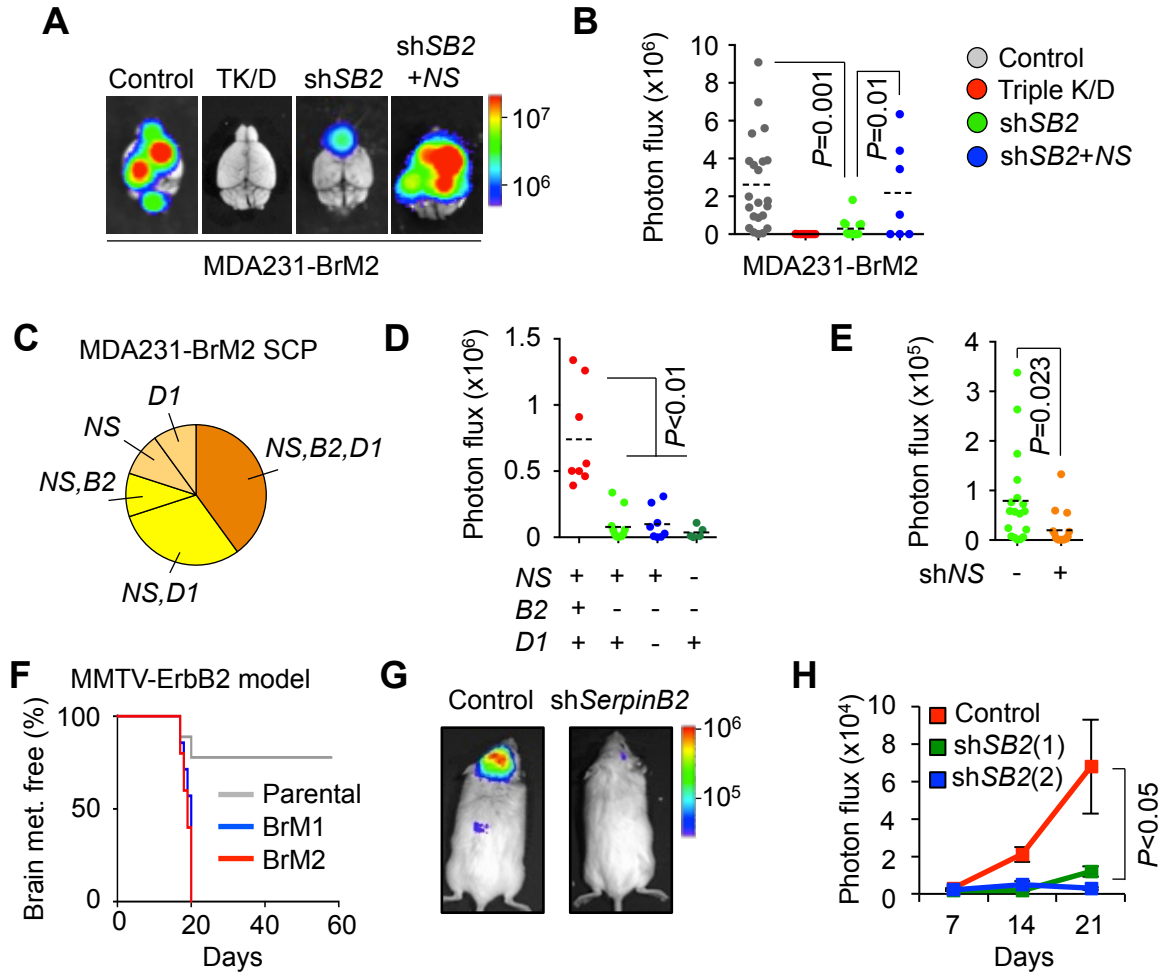
A

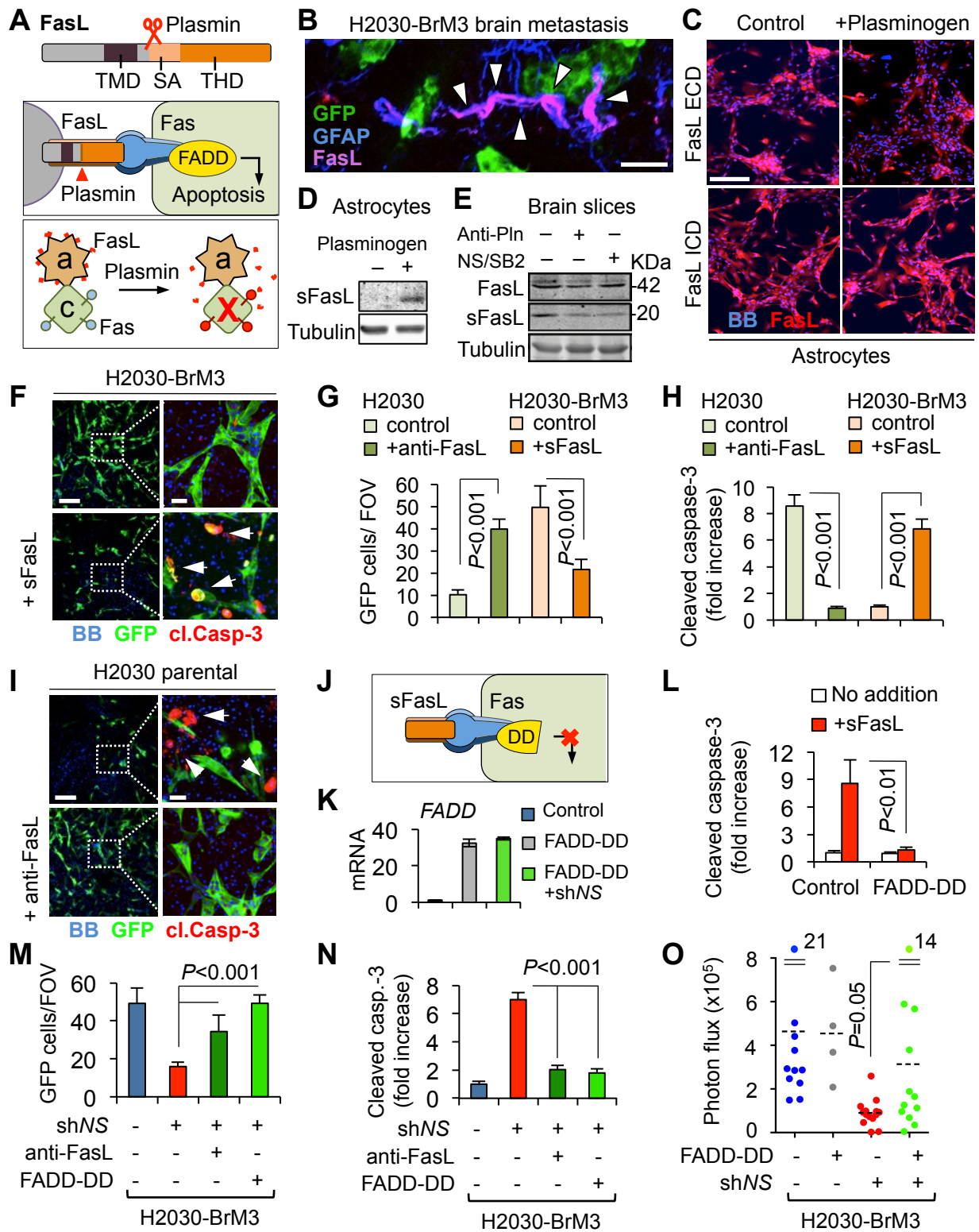
Cell line	Species	Tumor type	Source	Serpins mRNA (relative level)			
				I1 (NS)	B2	E2	D1
H2030-BrM3	Human	Lung adenocarcinoma (KRAS mutant)	Lymph node	3.4	0.3	1.4	0.3
PC9-BrM3	Human	Lung adenocarcinoma (EGFR mutant)	Lymph node	1.2	0.7	0.8	2.8
MDA231-BrM2	Human	TN breast carcinoma (ER-, PR-, HER2-)	Pleural fluid	5.0	10.1	0.5	5.1
CN34-BrM2	Human	TN breast carcinoma (ER-, PR-, HER2-)	Pleural fluid	8.9	15.5	9.6	8.5
Kras/p53-482N1	Mouse	Lung adenocarcinoma (Kras mutant, p53 null)	Lymph node	4.3	2.9	37.6	62.2
ErbB2-BrM2	Mouse	Breast carcinoma (ErbB2 hyperactive)	Mammary tumor	0.5	15.7	1.9	7.0

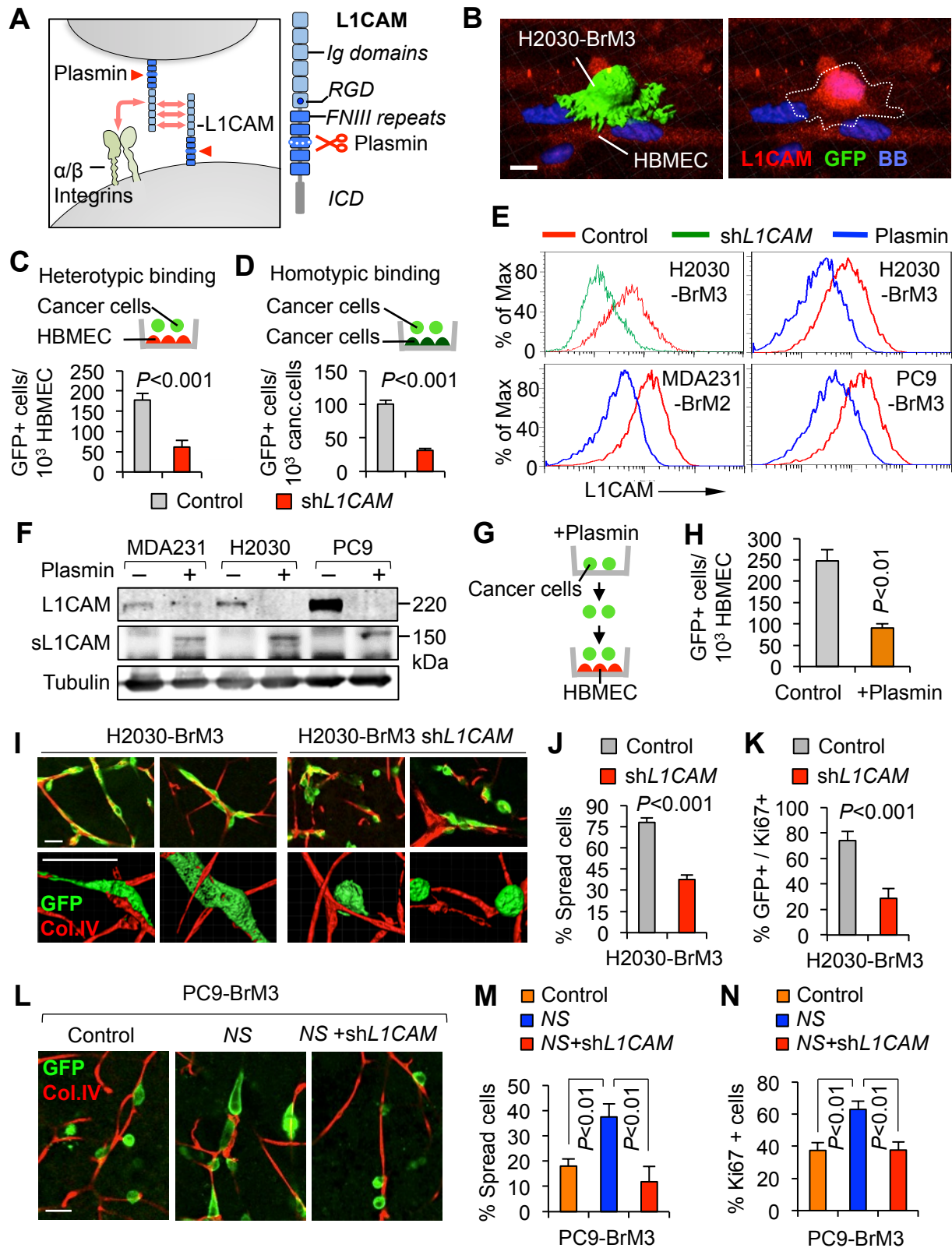


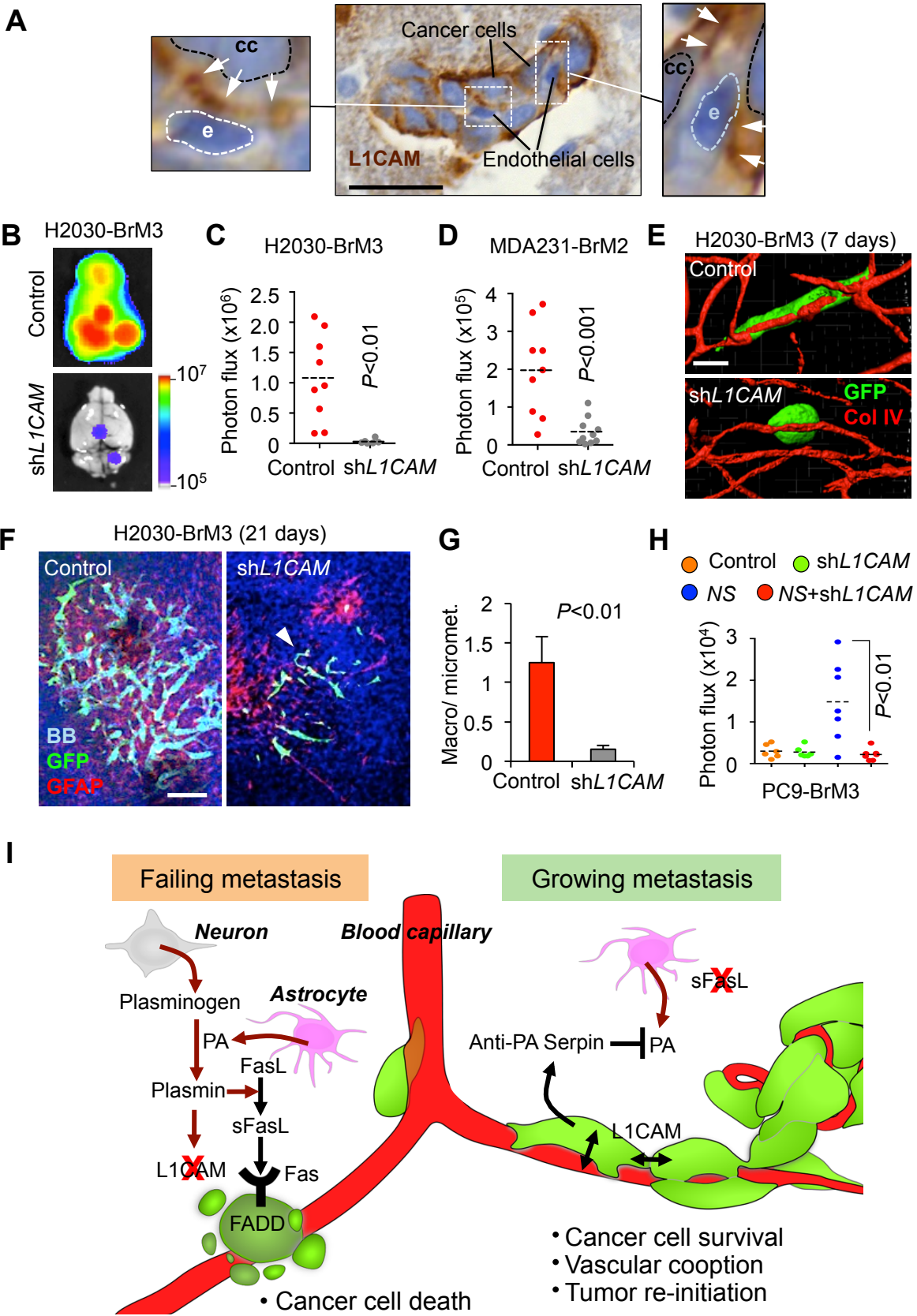


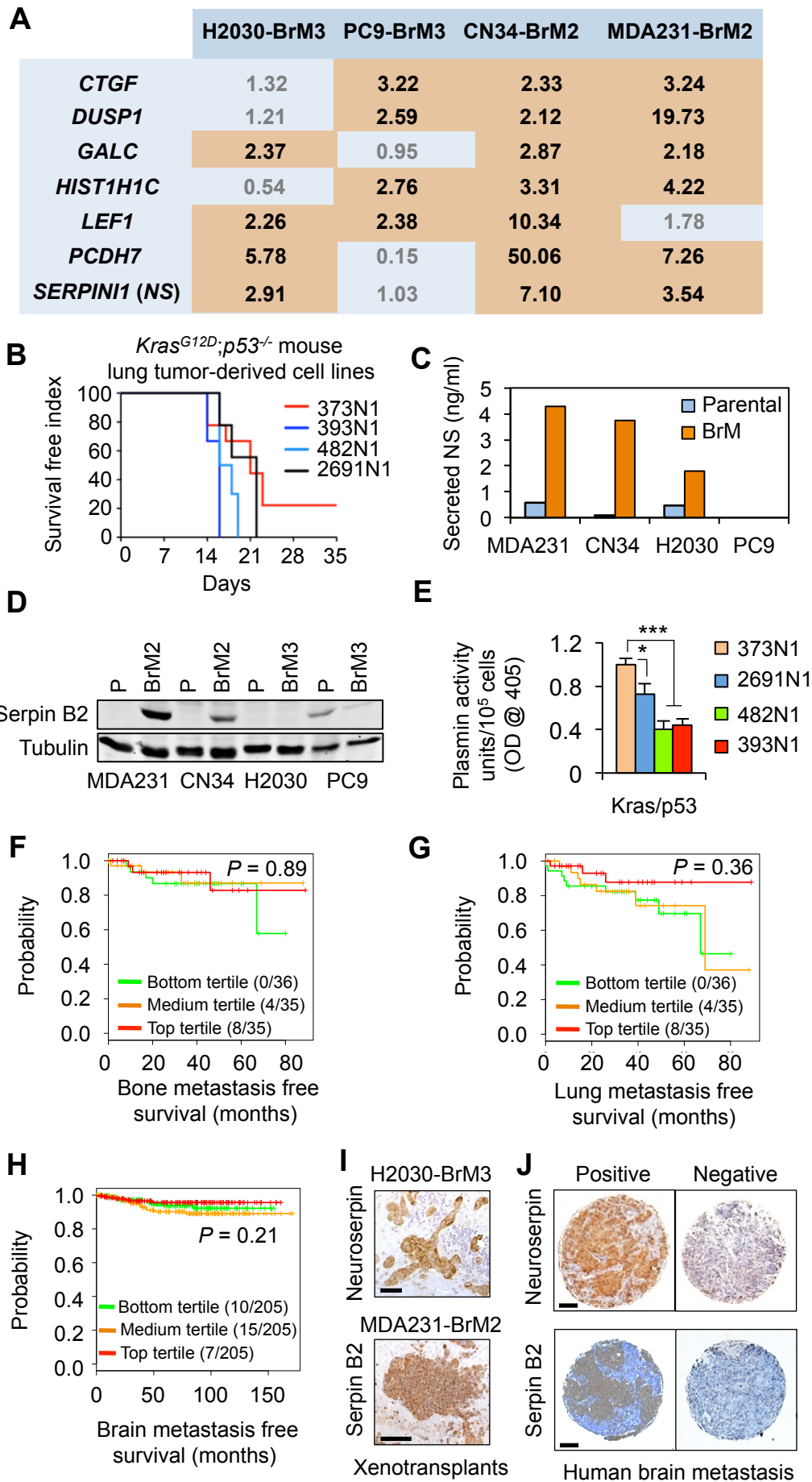




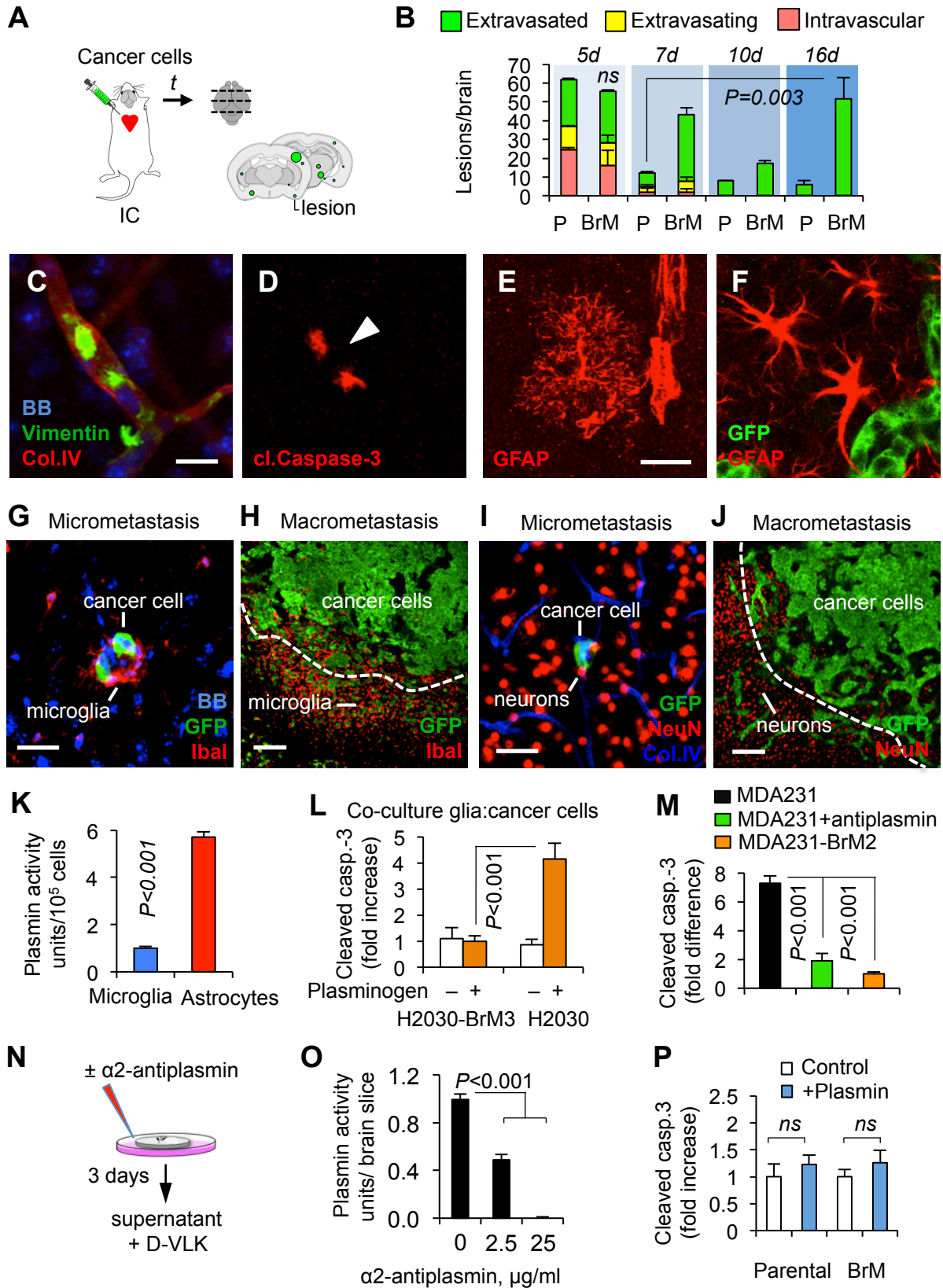




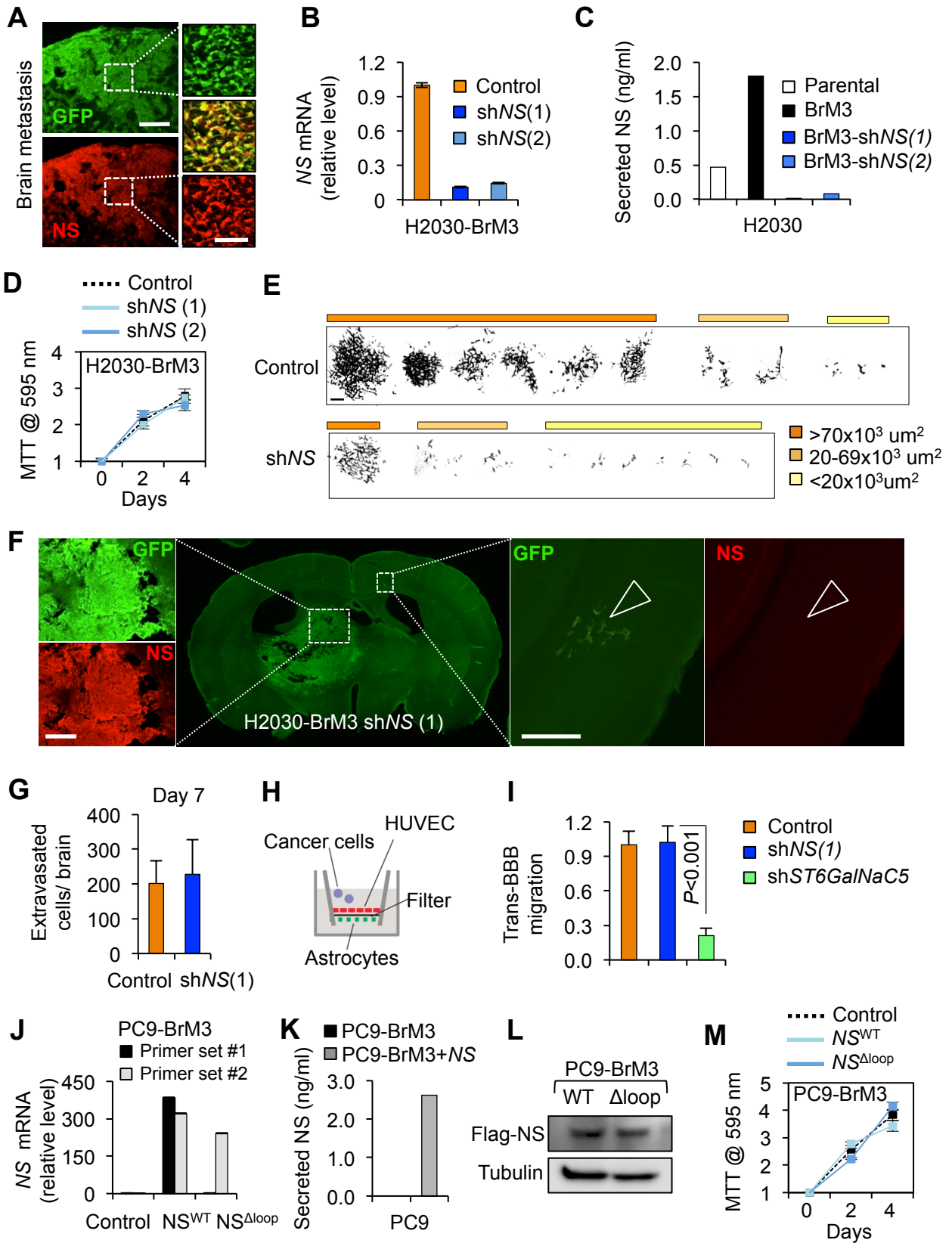




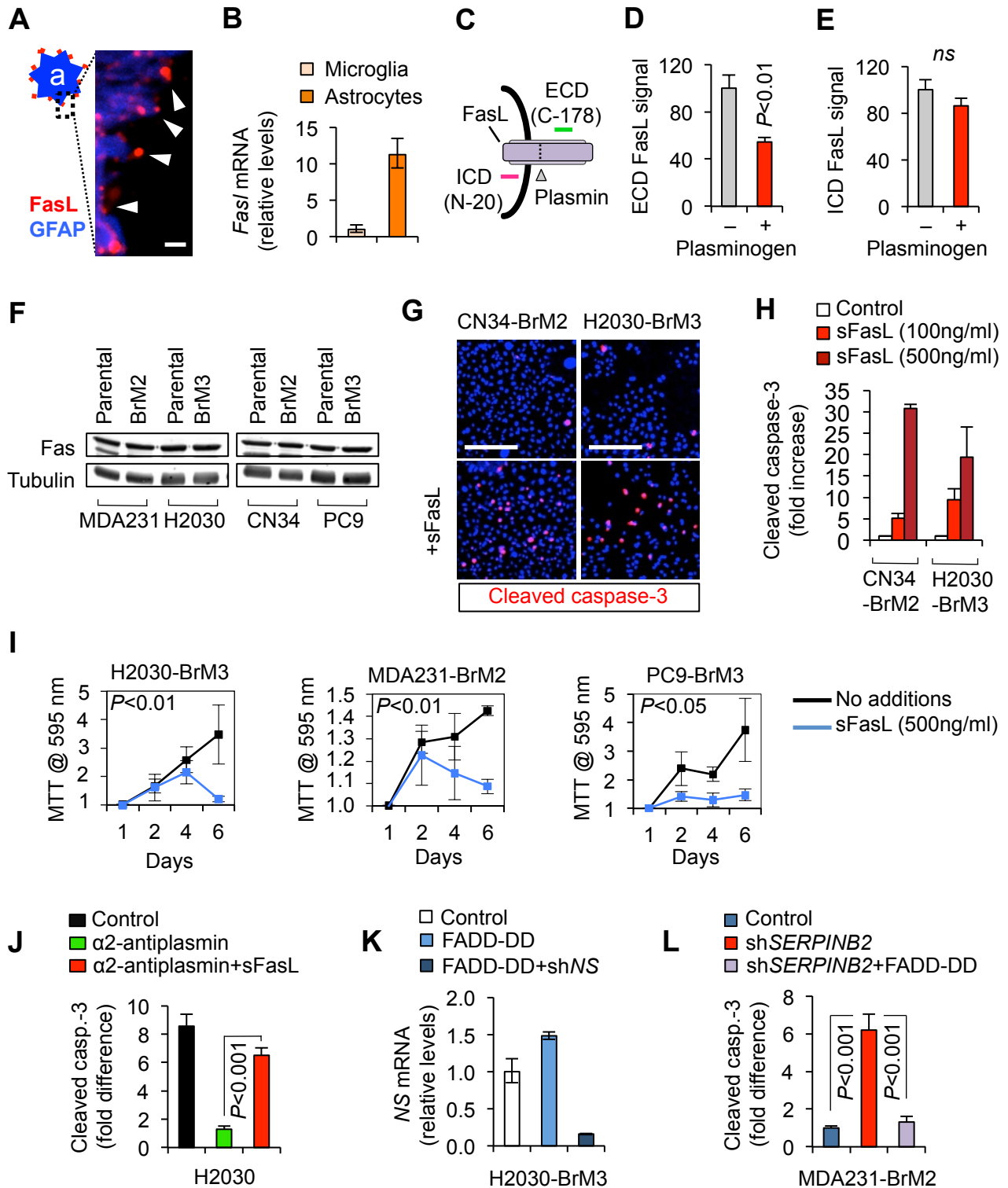
Valiente et al. Figure S1



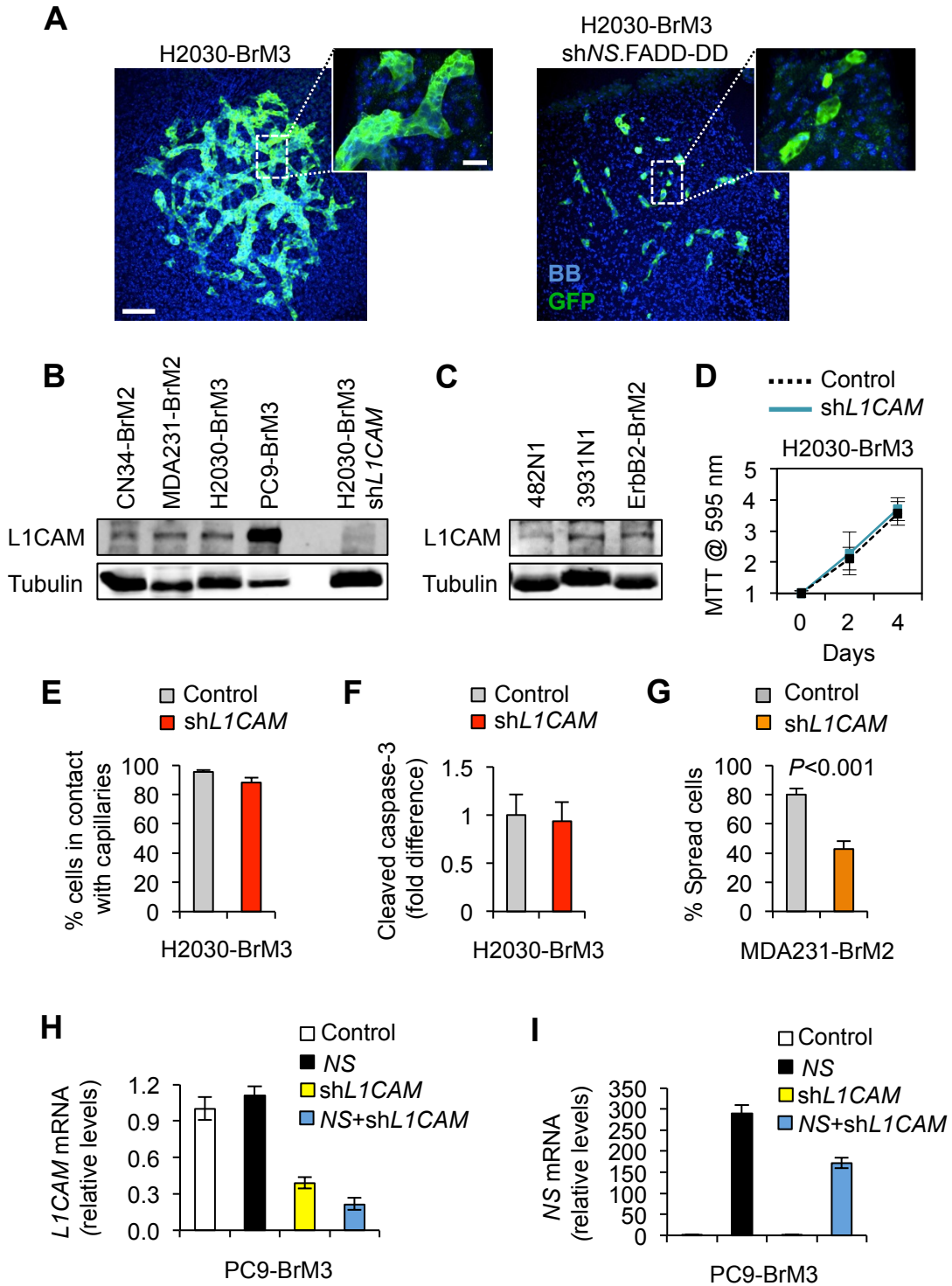
Valiente et al. Figure S2



Valiente et al. Figure S3

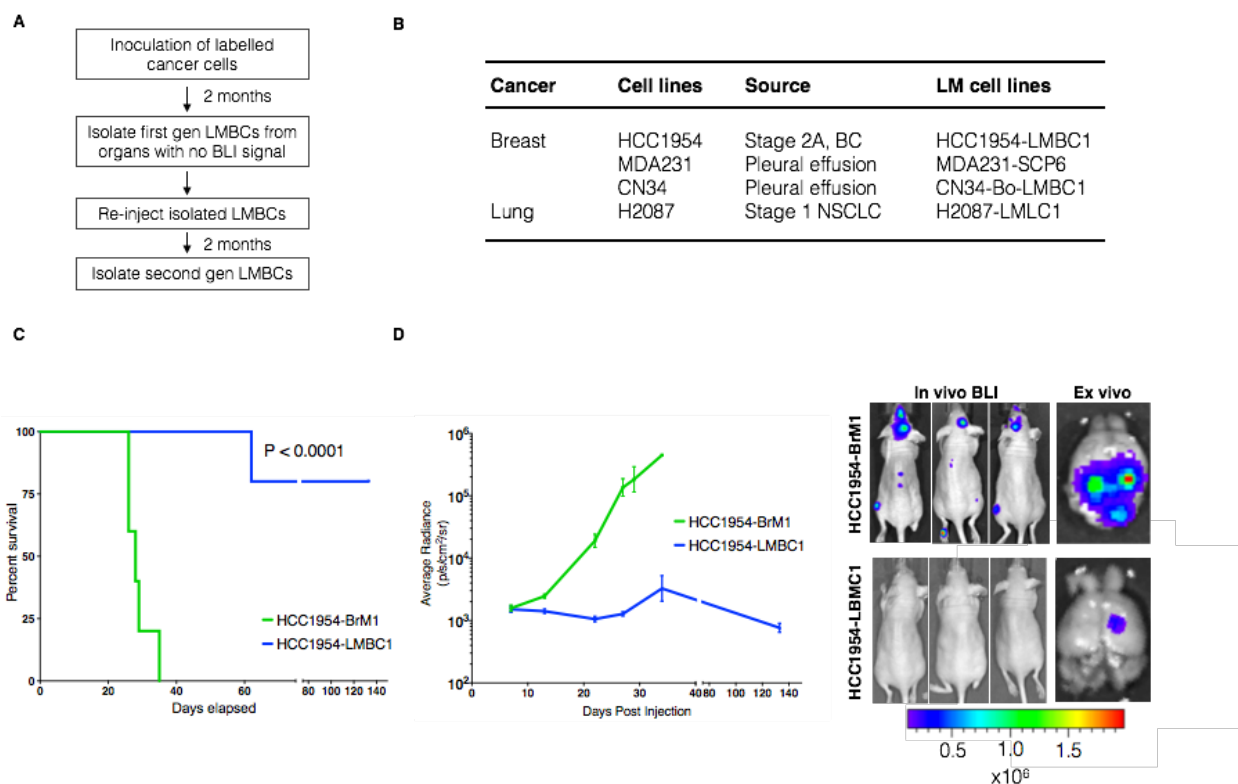


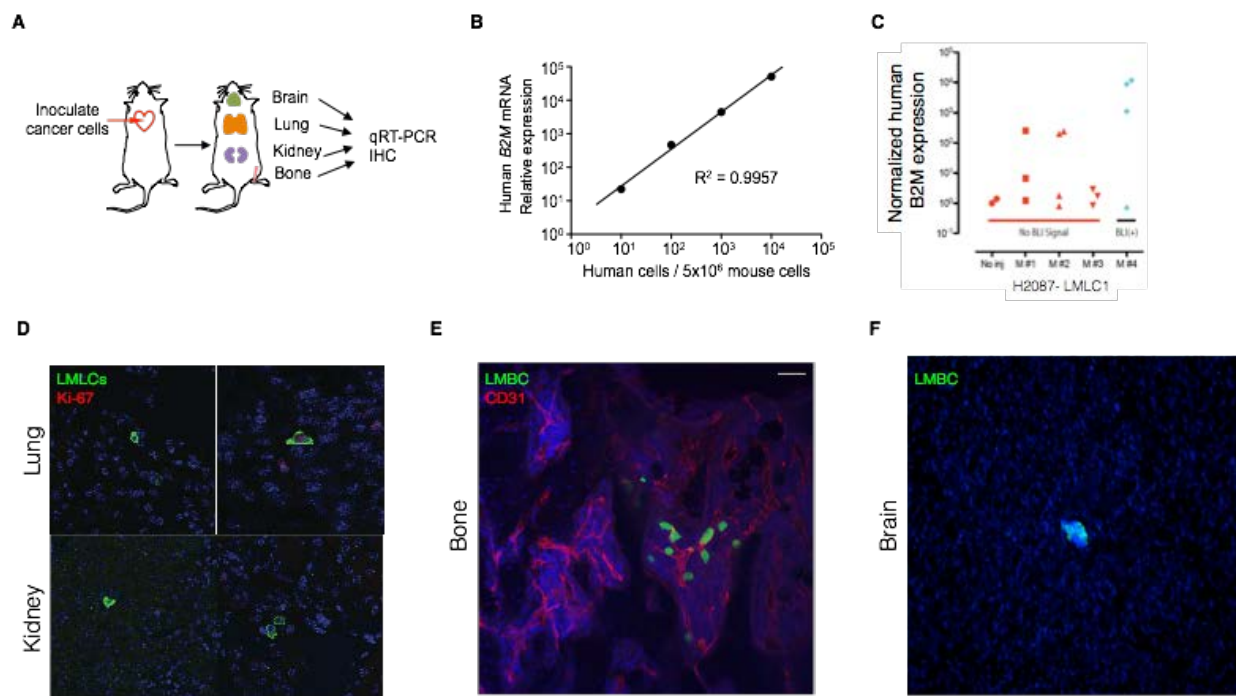
Valiente et al. Figure S5



Valiente et al. Figure S6

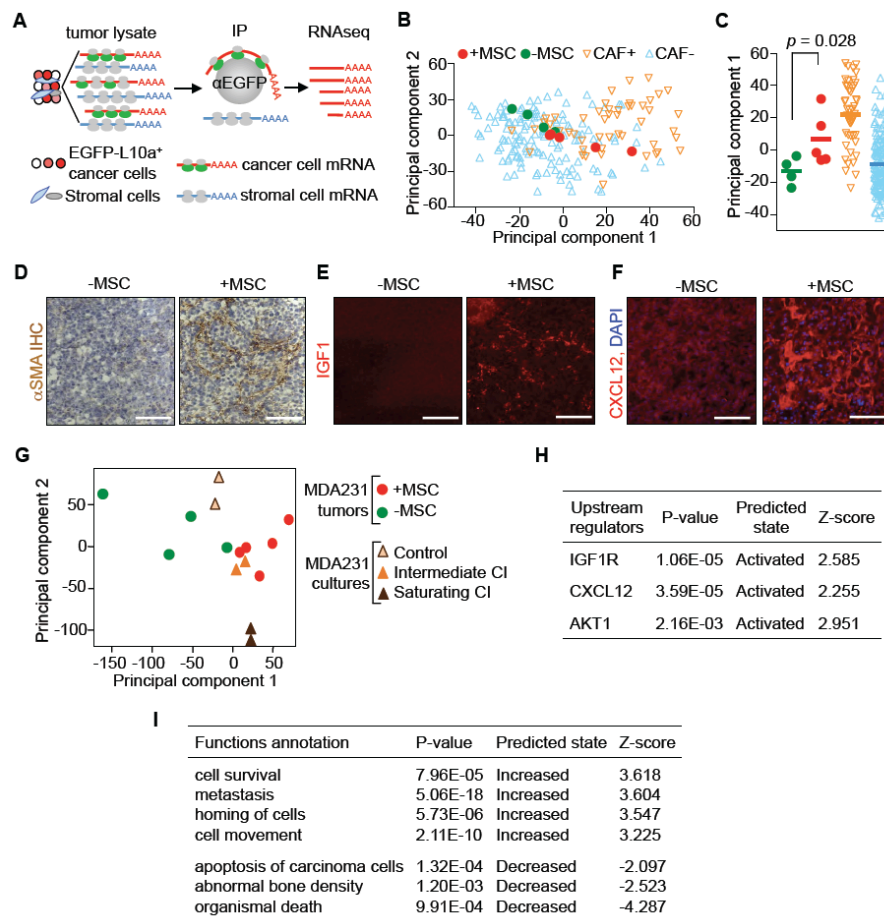
SUPPORTING DATA





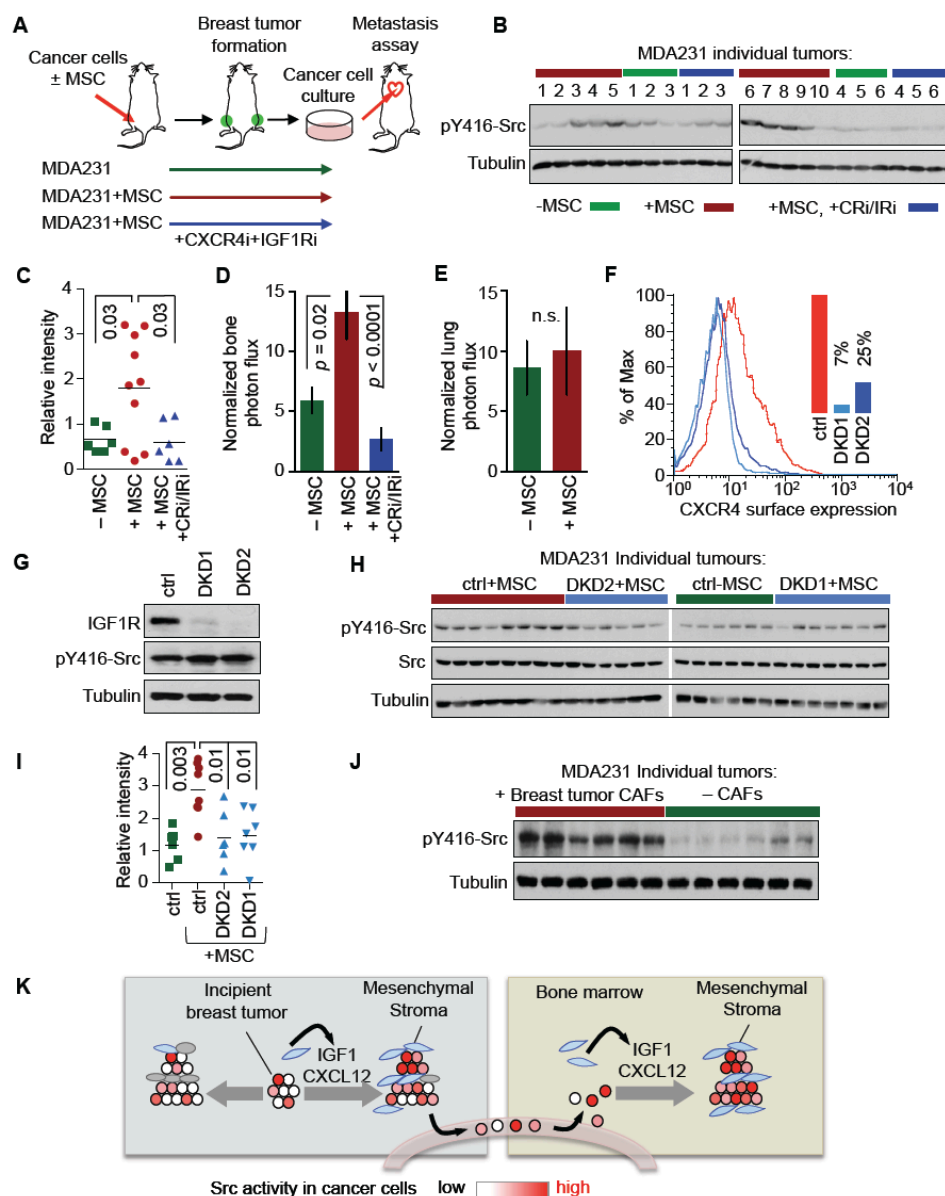
Supporting Figure 2. Detection of latent disseminated cancer cells.

(A) Detection of low abundance disseminated cancer cells from various mouse organs 2 months post intra-cardiac injections by qRT-PCR and IHC. (B) CN34 cells were serially diluted and spiked in 5×10^6 mouse bone marrow cells. RNA extraction was performed on these cell mixtures, followed by qRT-PCR. Human *B2M* expression was normalized against mouse *Actb* mRNA. Linear regression is plotted. (C) Lungs were isolated from mice with no BLI signal two months after injecting H2087-LMLC1 and qRT-PCR was performed using human specific *B2M* primer to detect LMLC1 cells. (D) IHC images of disseminated H2087-LMLC1 in the lung and kidney 2 months post intra-cardiac injection. Green: GFP, cancer cells; red: ki-67; blue: DAPI. (E) IHC image of disseminated MDA231-SCP6 cancer cells in the bone marrow. Green: GFP, cancer cells; red: CD31, blood vessel; blue: DAPI. (F) IHC image of disseminated HCC1954-LMBC1 in the brain 5 months post intra-cardiac injection. Green: GFP, cancer cells; blue: DAPI.



Supporting Figure 3. Tagged ribosome affinity purification (TRAP) demonstrates a transcriptional shift in mammary tumors under a mesenchymal stroma.

(A) Isolation of cancer cell-specific, polysome-associated transcripts by TRAP for RNA-seq analysis. (B-C) Principal component analyses of polysome-associated transcriptomic data of MDA231 from xenograft tumors and transcriptomic data of TN tumors from a clinical cohort. MDA231 mammary tumors were formed with MSC supplementation (+MSC) or without (-MSC) supplementation; TN tumors scoring as CAF+ or CAF- based on the CAF signature were from the EMC-MSK cohort. Principal component 1 maximally separates CAF+ from CAF- tumors and was used to generate the plot in (C). p value was calculated with t-test. (D-F) Histological analysis of mammary tumors generated with or without admixed MSCs. (D): Immunohistochemical (IHC) staining of α SMA (E): Immunofluorescent (IF) staining of IGF1. (F): IF staining of CXCL12, and DAPI nuclear staining. Scale bars, 100 μ m. (G) Principal component analysis using combined data of TRAP RNA-seq of MDA231 in vivo mammary tumors and that of in vitro CXCL12+IGF1 treatment (Figure 3C). The results show that intermediate CI samples fall closest to MSC+ tumors. Saturating CI samples, on the other hand, are dissimilar. Intermediate CI, intermediate [CXCL12, IGF1]; saturating CI, saturating [CXCL12, IGF1], refer to Figure 3C. (H-I) Ingenuity pathway analysis of the differentially expressed genes from polysome-associated transcriptomic data of MDA231 mammary tumors in (A-C). IGF1, CXCL12 and AKT signaling are predicted to be activated based on upstream regulator analysis (H). Metastasis-related biological processes are enriched (I).



Supporting Figure 4. Mesenchymal stroma selects bone metastatic cells in breast tumors

(A) Experimental strategy: MDA231 cells alone or admixed with MSCs were implanted in mammary fat pads. One set of mice was treated with CXCR4 inhibitor (CRi, AMD3100) and IGF1R inhibitor (IRi, BMS754807). After reaching 1cm³, tumors were excised and cancer cells were recovered and expanded in culture for testing. (B-C) pY416-Src levels in cancer cell lines from individual mammary tumors formed by MDA231 under the indicated conditions; immunoblot (B) and quantification (C). (D-E) Bone metastasis (D) and lung colonization (E) activity of the pooled cell lines derived in (B). Normalized bioluminescence signals were quantified at 21 days (D) or 30 days (E) after inoculation. Error bars = SEM, n = 8-10 in each group. (F) Flow cytometry analysis of CXCR4 surface expression in MDA231 with two independent double-knockdown (*DKD1*, *DKD2*) of *CXCR4* and *IGF1R* compared to control (*ctrl*). (G) Western immunoblot analysis of IGF1R and pY416-Src protein levels in two DKD

cell lines. (H-I) pY416-Src levels in cancer cell lines from mammary tumors formed by control MDA231 (*ctrl*) or two DKD cell lines with or without MSC supplementation; immunoblot (H) and quantification (I). (J) pY416-Src levels of cancer cell lines from individual mammary tumors formed by MDA231 cells with or without admixed CAFs from a human breast tumor. (K) A model of bone metastasis seed pre-selection by a mesenchymal-rich stroma in the mammary tumor. Blue and grey cells represent mesenchymal and non-mesenchymal stromal cells, respectively. As the tumor grows in a mesenchymal-rich microenvironment, the cancer cell population is skewed towards a preponderance of clones that thrive on mesenchymal cytokines such as CXCL12 and IGF1, which selects for a predisposition to metastasize in CXCL12- and IGF1-rich bone marrow.